Title: Hypoxic memory of tumor intrinsic type I interferon suppression promotes breast cancer metastasis

Authors: Oihana Iriondo[1,2,*#†], Desirea Mecenas[1,2*], Yilin Li[1,2,3*], Christopher R. Chin[4], Amal Thomas[5], Yonatan Amzaleg[1,2,6], Aidan Moriarty[1,7,8], Veronica Ortiz[1,2], Matthew MacKay[1], Amber Dickerson[1,2], Grace Lee[1,2], Sevana Harotoonian[1], Bérénice A. Benayoun[2,5,9], Andrew Smith[5], Christopher Mason[4], Evanthia T. Roussos Torres[2,10], Remi Klotz[1,2,7,8], Min Yu[1,2,7,8#]

Affiliations: [1]Department of Stem Cell Biology and Regenerative Medicine, Keck School of Medicine of the University of Southern California, Los Angeles, CA 90033, USA.

[2]USC Norris Comprehensive Cancer Center, Keck School of Medicine of the University of Southern California, Los Angeles, CA 90033, USA

[3]Key Laboratory of Carcinogenesis and Translational Research (Ministry of Education), Peking University Cancer Hospital and Institute, Beijing, China

[4]Department of Physiology and Biophysics, Weill Cornell Medicine, New York, NY 10021, USA

[5]Department of Molecular and Computational Biology, USC Dana and David Dornsife College of Letters, Arts and Sciences, University of Southern California, Los Angeles, CA 90089, USA

[6]Center for Craniofacial Molecular Biology, Ostrow School of Dentistry of the University of Southern California, Los Angeles, CA 90033, USA.

[7]Department of Pharmacology, University of Maryland School of Medicine, Baltimore, MD 21201, USA

[8]Marlene and Stewart Greenebaum NCI Comprehensive Cancer Center, University of Maryland School of Medicine, Baltimore, MD 21201, USA

24 [9]Leonard Davis School of Gerontology, University of Southern California, Los Angeles, CA
25 90089, USA

26 [10]Department of Medicine, Keck School of Medicine of the University of Southern California,
27 Los Angeles, CA 90033, USA.

28 **Running title:** Hypoxic memory of IFN/AP suppression promotes metastasis

29 **Keywords:** Circulating tumor cells, metastasis, hypoxia, hypoxic memory, type I interferon

30

31 **Additional information:**

32 Financial support: The National Institutes of Health (NIH) grant DP2 CA206653 (M.Y.), the
33 Stop Cancer Foundation (M.Y.), the PEW Charitable Trusts and the Alexander & Margaret
34 Stewart Trust (M.Y.), the Department of Defense Era of Hope Scholar Award (M.Y.), the
35 Richard Merkin Foundation (M.Y.), the Broad Fellowship (O.I.), and the NIH grant
36 T90DE021982 (trainees D.M. and Y.A.). The project described was supported in part (core
37 facilities) by award number P30CA014089 from the National Cancer Institute.

38

39 [#]Corresponding authors: Min Yu, 655 West Baltimore St, Bressler Research Building, Rm 10-
40 043, Baltimore, MD 21201. Phone: (410) 706-6479. Email: Min.Yu@som.umaryland.edu and
41 Oihana Iriondo, email: oiriondo@cicbiogune.es

42

43 [†]Present affiliations: CIC bioGUNE, Bizkaia Technology Park, Derio 48160, Spain. Ikerbasque,
44 Basque Foundation for Science, Bilbao, Spain.

45 [*]Oihana Iriondo, Desirea Mecenas, and Yilin Li contributed equally to this work.

46

47 Disclosure of potential conflicts of interest: M. Yu. is the founder and director of CanTraCer

48 Biosciences Inc.

Abstract

Hypoxia is a common feature of many solid tumors due to aberrant proliferation and angiogenesis and has been associated with tumor progression and metastasis. Most of the well-known hypoxia effects are mediated through hypoxia-inducible factors (HIFs), but the long-lasting effect of hypoxia beyond the immediate HIF regulation remains less understood. Here we show that hypoxia exerts a prolonged effect to promote metastasis. Using breast cancer patient-derived circulating tumor cell (CTC) lines and common breast cancer cell lines, we found that hypoxia downregulates tumor intrinsic type I interferon (IFN) signaling and its downstream antigen presentation (AP) machinery in luminal breast cancer cells, via both HIF-dependent and HIF-independent mechanisms. Hypoxia induced IFN/AP suppression can last longer than the hypoxic exposure, presenting a "hypoxic memory" phenotype. Hypoxic memory of IFN/AP downregulation is established by specific hypoxic priming, and cells with hypoxic memory have an enhanced ability for tumorigenesis and metastasis. The histone deacetylase inhibitor (HDACi) Entinostat can erase the hypoxic memory and improve the immune clearance of tumor cells when combined with checkpoint immunotherapies in a syngeneic breast cancer mouse model. These results point to a novel mechanism for hypoxia facilitated tumor progression, through a long-lasting memory that provides advantages for CTCs during the metastatic cascade.

Significance: We revealed a novel hypoxic memory of prolonged suppression of tumor intrinsic type I IFN and AP signals that promote tumorigenesis and metastasis, suggesting novel mechanistic understanding of the immune evasive properties of CTCs.

70 **Introduction**

71

72 In solid tumors, rapid cell division and aberrant angiogenesis often lead to oxygen deprivation or
73 hypoxia, which has long been associated with increased malignancy, poor prognosis, and
74 resistance to radio- and chemotherapy(1). Hypoxia influences tumor progression through a
75 variety of mechanisms (reviewed in(2)), including promotion of angiogenesis(3), matrix
76 remodeling(4), enhanced cell motility and cancer stem cell content(5–7), and modification of the
77 premetastatic niche(8,9). Hypoxia-inducible factors (HIFs) play a central role in many of these
78 processes. HIFs are heterodimers composed of an oxygen labile alpha subunit (HIF1α, HIF2α,
79 or the lesser known HIF3α) and a stable beta subunit (HIF1β, also known as ARNT). Under well
80 oxygenated conditions, HIF1α and HIF2α are hydroxylated in two conserved proline residues by
81 EGLN proteins (also known as prolyl hydroxylases, PHDs), bound by the von Hippel-Lindau
82 (VHL) protein and targeted for proteasomal degradation(10–12). PHDs belong to the 2-
83 oxoglutarate-dependent dioxygenase (2OGDD) superfamily and use O_2 as a co-substrate.
84 Therefore, when oxygen availability is low HIFα is stabilized, binds to HIF1β and regulates the
85 expression of a myriad of genes involved in proliferation, metabolism, cell motility, apoptosis,
86 etc.(13,14). Several studies have underscored the importance of alternative HIF-independent
87 mechanisms in regulating the cellular response to hypoxia. Besides HIFα, PHDs can hydroxylate
88 non-HIFα substrates in an oxygen-dependent manner, regulating their stability or activity(15). In
89 addition, other enzymes from the 2OGDD superfamily of proteins have been shown to function
90 as oxygen sensors, including TET DNA demethylases(16) and several Jumonji (JmjC) histone
91 demethylases (KDMs)(17,18). Furthermore, some TET and JmjC-KDMs are transcriptionally

92 regulated by HIF(19), highlighting a complex role for hypoxia in shaping the epigenetic
93 landscape of cells.

94

95 Tumor hypoxia has been linked to immunosuppression (20,21). Hypoxic areas in tumors attract
96 M2-like tumor associated macrophages (TAMs)(22,23), myeloid-derived suppressor cells
97 (MDSCs)(24) and regulatory T cells (Tregs), and show reduced CD8 T cell infiltration(25).
98 Furthermore, hypoxic microenvironments can lead to diminished T cell performance and
99 survival, mostly due to metabolic alterations driven by hypoxia, such as increases in lactic acid
100 and extracellular adenosine(20,26). However, the effect of hypoxia on tumor cell intrinsic
101 immune evasive features are less characterized.

102

103 A key class of cytokines that play pivotal roles in the immune response against infectious agents
104 and tumors are type I interferons (IFNs)(27). Type I IFNs are a family of protein consisting of 13
105 IFNα subunits, IFNβ, and several poorly defined single gene products(28). Expression of type I
106 IFNs is induced by the activation of pattern and danger recognition receptors. Once secreted,
107 IFNs signal through the IFNα/β receptor (IFNAR, composed of subunits IFNAR1 and IFNAR2),
108 which phosphorylates JAK1 and TYK2, resulting in phosphorylation and activation of
109 STAT1/STAT2 heterodimers. Phosphorylated STAT1/STAT2 bind to IRF9 to form the
110 interferon-stimulated gene factor 3 (ISGF3). ISGF3 translocates to the nucleus and binds to
111 interferon signaling response elements (ISRE) to induce the expression of interferon stimulated
112 genes (ISGs). In addition to this canonical signaling, type I IFNs can activate signaling by
113 STAT3-6, JNK, ERK, MAPK and mTOR pathways(28). Type I IFNs can regulate tumor growth

114 directly – by impacting cell proliferation and survival – or indirectly – by modulating antitumor
115 immunity or influencing tumor angiogenesis(29).
116
117 Our previous work has shown that the hypoxia signaling pathway is significantly upregulated in
118 CTCs isolated from patient blood during disease progression compared to those isolated during
119 treatment response(30). Hypoxia is a condition that facilitates the establishment of CTC
120 lines(30,31) with the capacity to metastasize to the major organs of experimental mice, as seen in
121 the corresponding patients(32). Furthermore, recent reports showed that hypoxia promotes CTC
122 generation and pro-metastatic behavior(33,34). It has been clear that hypoxia induced molecular
123 changes could play important roles in promoting metastasis. However, the long term effect of
124 hypoxia in CTCs that exited the exposure has not been fully characterized.
125
126 **Results**
127 **Hypoxia downregulates IFN and AP pathways in luminal breast cancer cells.**
128 To test if hypoxic cultures impact the tumor formation and metastatic capacity of CTC lines, we
129 grew GFP-LUC labeled CTCs for 8 weeks in normoxic or hypoxic cultures, and then injected
130 them into the mammary fat pads or the tail veins of NSG mice (Figure 1A). Once the CTC lines
131 are established, normoxic culture did not decrease cell growth (Figure S1A) nor significantly
132 affect cell death (Figure S1B). *In vivo*, BRx50 and BRx68 CTC lines formed larger tumors after
133 being cultured in hypoxia compared to normoxia, while BRx07, BRx42 and BRx61 cells formed
134 similarly sized tumors following culture in both conditions (Figures 1B and S1C). In the setting
135 of experimental metastasis via tail vein injection, 7 out of 10 mice injected with BRx68 cells
136 grown in hypoxic conditions showed metastatic signals detected by bioluminescent imaging 14

137 weeks after injection, compared to only 1 out of 7 mice injected with BRx68 cells grown in
138 normoxia (Figures 1C and S1D). In contrast, mice injected with BRx07 cells cultured in
139 normoxia or hypoxia showed similar levels of metastasis (Figure S1E).
140
141 RNA-seq analysis of BRx68 cells cultured in normoxia or hypoxia for 8 weeks showed 84 genes
142 upregulated and 241 genes downregulated in hypoxia (fold change≥1.5, FDR≤0.05) (Figure 2A;
143 Table S1-S2). Pathway analysis of these differentially expressed genes showed an enrichment for
144 immune related pathways, especially interferon (IFN) signaling and the antigen presentation
145 (AP) pathway. All genes in these pathways showed lower expression in hypoxia (Figure 2B).
146 Similarly, Gene Set Enrichment Analysis (GSEA) with genes downregulated in hypoxia showed
147 significant overlaps with several gene sets involved in interferon response (Table S3). As
148 expected, the list of genes upregulated in hypoxia significantly overlapped with several hypoxia
149 gene sets (Table S4). qPCR analysis confirmed the lower expression of the IFN target genes
150 ISG15, IFIT1 and IFIT3 in BRx68 cells grown in hypoxia and showed similar results with
151 BRx07 and BRx50 cells (Figure 2C). Flow cytometry analysis of the MHC-I molecules in
152 BRx68 and BRx50 also showed significantly reduced levels in cells cultured in hypoxia,
153 compared to those cultured in normoxia for 8 weeks (Figure 2D).
154
155 We next set out to determine whether hypoxia reduces the expression of IFN target genes in
156 other breast cancer cell lines. In response to hypoxia, all human cell lines tested upregulated the
157 HIF target genes CA9 and PHD3 (Figure 2E). However, hypoxia reduced IFIT1 and ISG15
158 expression in MCF7, T47D and BT474 cells, while failing to do so in MDA-MB-231 and
159 HS578T cells (Figure 2E). We also tested mouse mammary tumor cell lines in hypoxia, and

160 found reduced Ifit1 and Isg15 expression levels in Py117(35) and NT2.5(36) cells, but not in
161 Py8119(35) cells (Figure 2F). To investigate the molecular characteristics distinguishing cells
162 that decrease IFN target gene expression in hypoxia (responders) from those that do not (non-
163 responders), we analyzed publicly available RNA-seq datasets of human breast cancer cell lines
164 and microarray data from mouse cell lines. Genes differentially upregulated in responders
165 showed significant overlap with several sets of genes upregulated in luminal tumors (compared
166 to basal tumors) and genes downregulated during epithelial to mesenchymal transition (EMT)
167 (Tables S5). In contrast, genes overexpressed in non-responders overlapped significantly with
168 sets of genes downregulated in luminal tumors and genes upregulated during EMT (Tables S6).
169
170 To evaluate whether the same patterns also presented *in vivo*, we next investigated whether
171 tumors from breast cancer patients showed inverse correlations between a hypoxia signature(37)
172 and a signature composed of genes from the IFN and AP pathways that were differentially
173 expressed in our RNA-seq analysis (IFN/AP signature) (Figure 2A; Table S7). Most breast
174 tumors in the TCGA dataset had low scores for both signatures. However, tumors with high
175 scores for the hypoxia signature generally showed low scores for the IFN/AP signature, and vice-
176 versa (Figures 3A and S2A). Since TCGA datasets are obtained from bulk tumors, the inverse
177 correlation between hypoxia and IFN/AP signatures could be a consequence of the differential
178 recruitment of immune cells to hypoxic vs. non-hypoxic tumors. To explore possible correlations
179 between these 2 signatures in tumor cells *in vivo*, we performed single-cell RNA sequencing
180 (scRNAseq) analysis of spontaneous breast tumors formed in the FVB-MMTV-PyMT mouse
181 model. Using the same mouse model, another group reported that about 2 percent of tumor tissue
182 dissected from 11-weeks-old mice and 10 percent from 16-weeks-old mice were hypoxic(38).

183 Taking this into consideration, tumors from two 12-week-old and two 16-week-old mice were
184 dissociated, and cells were subjected to scRNAseq using the Chromium platform. Using Seurat,
185 we first annotated clusters representing different cell types found in the tumor (Figure S2B), and
186 then projected the hypoxia and IFN/AP signatures on the tumor cells (Figure S2C). For each time
187 point, tumor cells were arranged in deciles according to their IFN/AP scores (Figure 3B). The
188 hypoxia scores for the corresponding tumor cells in each decile showed an inverse correlation
189 with the IFN/AP scores at the earlier time point (12 weeks), but a positive correlation at the later
190 time point (16 weeks) (Figures 3B and S2D). This was consistent with our *in vitro* finding, given
191 reports that the MMTV-PyMT model progresses with a loss of luminal features over time(39).
192 We also applied the same analysis to a published scRNAseq dataset that includes several
193 syngeneic tumor models(40), and found that all 4 models showed a clear inverse correlation of
194 hypoxia and IFN/AP signatures in Cd24-sorted tumor cells (Figure 3C).
195
196 **Hypoxic memory of prolonged suppression of IFN/AP is associated with enhanced tumor**
197 **progression.**
198 Intrigued by the differences between BRx07 and BRx68 *in vivo*, we assessed the stability of the
199 hypoxia-induced downregulation of IFN target genes upon reoxygenation. In both BRx07 and
200 BRx68 cells, 3-day reoxygenation results in complete loss of HIF1α expression and decreases
201 HIF target gene expression to same levels as those found after reoxygenation for 7 days (Figures
202 S3A-F). Interestingly, a 3-day reoxygenation period is sufficient to significantly increase IFIT1
203 and IFIT3 expression levels in BRx07 cells, but not in BRx68 cells (Figures 4A and S3C, S3F).
204 In fact, the increase in IFN target genes observed in BRx07 cells reoxygenated for 3 days was
205 bigger than the increase in cells reoxygenated for 8 weeks (2.9x vs 1.6x for IFIT1, 4x vs 1.75x

206 for IFIT3) (Figure 4A). In BRx68 and BRx50 cells, the increase in IFN target gene expression
207 was only observed when cells were reoxygenated for 8 weeks (Figures 4A and S3G).
208 Accordingly, tumors formed by BRx68 cells grown in normoxia for 3 days were significantly
209 bigger than those formed by cells grown in normoxia for 8 weeks (Figure 4B). Similar
210 maintenance of IFN pathway suppression was also observed in HLA-ABC levels in BRx68 and
211 BRx50 after reoxygenation for 3 days (Figures 2D and S3H).
212
213 We next evaluated if the sustained suppression of IFN targets by hypoxia observed in CTC lines
214 also occurs in other breast cancer cell lines. When MCF7 cells were cultured in 4% or 1% O_2 for
215 14 days and then reoxygenated for 3 days (see Methods), cells that had been grown in 4% O_2
216 maintained lower IFN target levels, even though the HIF target PHD3 reached basal expression
217 levels (Figure 4C). Intriguingly, tumor growth in the mammary fat pads of NSG mice showed an
218 association with the prolonged suppression of the IFN target: MCF7 cells grown in hypoxia,
219 especially at 4% oxygen, for 14 days formed bigger tumors than those grown in normoxia
220 (Figure 4D). In contrast, a shorter exposure to hypoxia for 3 days did not maintain the
221 suppression of the IFN target ISG15 (Figure 4E), and MCF7 cells grown in various oxygen
222 conditions for 3 days produced similar sized tumors (Figure 4F). Taken together, these results
223 suggest that certain breast cancer cells can maintain lower IFN signaling even after they exit
224 hypoxic niches, suggesting the existence of a “hypoxic memory”.
225
226 **Both HIF-dependent and -independent mechanisms regulate IFN**
227 To clarify the mechanism by which hypoxia reduces IFN target gene expression in luminal breast
228 cancer cells, we first evaluated whether there are different levels of mitochondrial double strand

229 RNA (dsRNA), an endogenous IFN stimulus, as recently reported(41). Immunofluorescence
230 staining using the J2 antibody, which is commonly used to detect mitochondrial dsRNA, did not
231 detect a significant decrease of signal in MCF7 cells cultured in in 4% or 1% hypoxia for 3 days
232 compared to that in normoxia (Figure S4A). To test whether there were different responses to the
233 same stimulus, we transfected the MCF7 cells that have been cultured in different oxygen levels
234 for 14 days with the viral double stranded RNA analogue poly(I:C) (42) and grew them in the
235 normoxic condition for 6 additional hours before harvesting. We found that indeed the activation
236 of phospho-STAT1 in response to the poly(I:C) stimulus is dampened in cells cultured in
237 hypoxia (Figure S4B).
238
239 We then evaluated whether HIF activity is needed and used CRISPR-Cas9 to delete ARNT, the
240 HIF1α and HIF2α heterodimerization partner that is essential for the transcriptional activity of
241 HIFs(43). ARNT knockout (KO) in MCF7 cells led to the inability of hypoxia to induce the
242 expression of NDRG1, a target of both HIF1 and HIF2(44) (Figure 5A-B). However, IFN target
243 gene expression was reduced in response to hypoxia both in control and ARNT-KO cells
244 (Figures 5B and S4C), suggesting that the effect of hypoxia on IFN signaling can be observed
245 independent of HIF. Since there are reported PHD dependent but HIF-independent mechanism of
246 hypoxia influence (45), we next treated MCF7 cells with the PHD inhibitor FG4592(46) that led
247 to HIF1α stabilization and induction of HIF target genes in MCF7 (Figure S4D-E) and T47D
248 cells (Figure S4F-H), showing that the drug is efficient in inhibiting PHD activity. Cells treated
249 with this small molecule also exhibited lower expression of IFN target genes (Figures 5C and
250 S4G). Interestingly, in MCF7 ARNT-KO cells, treatment with FG4592 and DMOG, a 2-OG
251 analogue that leads to PHD inactivation and HIF1α stabilization (47) as unable to reduce IFN

252 target gene expression (Figure 5D), suggesting that the effect that inhibition of PHDs has on IFN
253 signaling is mediated by HIF. We then overexpressed mutated forms of HIF1α and HIF2α,
254 with mutations on two prolyl sites, that render them insensitive to regulation by PHDs in
255 normoxia (48), resulting in HIF1α and HIF2α stabilization (Figure S4I-J) and increased
256 expression of downstream targets (Figure 5E-F) in normoxia conditions . Intriguingly, while
257 mutant HIF1α overexpression suppressed the expression of IFN target genes (Figure 5E) mutant
258 HIF2a overexpression had the opposite effect (Figure 5E-F). These data indicate the existence of
259 both HIF1-dependent and HIF-independent mechanisms for downregulating IFN signaling.
260
261
262 We next investigated potential HIF-independent mechanisms for hypoxic suppression of IFN
263 signaling. Recent reports have shown that, similar to the PHDs that hydroxylate HIF in well
264 oxygenated environments, other proteins of the 2-oxoglutarate-dependent dioxygenase family,
265 including some histone demethylases, show low oxygen affinity (high K_M), enabling them to
266 sense physiological changes in oxygen(18,49). As a result, hypoxic culture decreases the activity
267 of such histone demethylases, leading to increased levels of methylation in several H3 residues
268 (Figure S5A). KDM6A, KDM5A and KDM4B are 3 of the histone demethylases with the
269 highest K_M for oxygen(18). To determine if inhibition of these histone demethylases can mimic
270 the effect of hypoxia on interferon target genes, we treated MCF7 cells with small molecule
271 inhibitors that specifically target these enzymes. Treatment with the KDM6 inhibitor GSK-
272 J4(50) increased H3K27 trimethylation, but actually enhanced IFN target gene expression
273 (Figures S5B-C). Similarly, MCF7 cells treated with the KDM5 inhibitor KDM5-C70(51) that
274 increases H3K4me3 showed small but significant increases in IFN target gene expression (Figure

275 S5D-E). The KDM4 inhibitor NSC636819(52) promoted a modest increase in H3K9me3 levels
276 (Figure S5F). NSC636819 treatment failed to mimic the effect of hypoxia on IFN target genes
277 (Figure S5G), although it did downregulate ESR1 and its target gene PS2 (Figure S5H), as
278 reported elsewhere(53,54). These data suggest that the reduced activities of KDMs are not
279 directly responsible for suppressing the IFN/AP signal.
280
281 **Hypoxic tracing plasmids allows validation of hypoxic memory *in vivo***
282 To elucidate whether such "hypoxic memory" can be found *in vivo*, we designed a 2-plasmid
283 reporter system that enables us to permanently mark cells exposed to hypoxia so that they can be
284 tracked during tumor progression (Figure 6A). Cells that express this 2-plasmid reporter system
285 are initially RFP positive but upon exposure to hypoxia, permanently lose RFP expression due to
286 gene excision and start expressing GFP. FACS analysis of MCF7 cells transduced with the 2-
287 plasmid reporter showed that, while the vast majority of cells remained RFP^+GFP^- when cultured
288 in normoxic conditions, an average of 56.7% of cells grown in hypoxia (1% O_2) for 3 days were
289 GFP^+ (Figure S6A-B). When the hypoxia tracing MCF7 (MCF7-HypT) cells were cultured in 3D
290 mixed matrigel/collagen gels, spheres that were originally exclusively RFP^+ developed GFP^+
291 areas as they grew, suggesting the system can detect local hypoxia in spheres (Figure S6C). We
292 next injected MCF7-HypT cells into the mammary fat pads of NSG mice. After 8 weeks, mice
293 were injected with the hypoxia detecting probe pimonidazole(55), and tumors and lungs were
294 dissected and fixed 90 minutes later. Immunostaining of tissue sections suggested that cells that
295 have been exposed to hypoxia were more efficient in metastasizing to the lung, since the
296 proportion of GFP^+ metastatic loci in lungs was significantly higher than the proportion of GFP^+
297 cells in primary tumors (Figures 6B and S6D-E). Importantly, immunofluorescence staining also

298 revealed that CRE expression was exclusively detected in pimonidazole-positive areas, while
299 GFP^+ cells could be detected in non-hypoxic areas, showing that many cells had exited hypoxic
300 niches after converting into GFP-expressing cells (Figure 6C. In fact, staining of whole tumor
301 sections demonstrated that the vast majority of GFP^+ cells were located in pimonidazole-negative
302 non-hypoxic regions of the tumor (Figure S6F). In accordance with our *in vitro* results, RFP^-
303 GFP^+ cells sorted from MCF7-HypT tumors showed lower expression levels of IFN target genes
304 than their RFP^+GFP^- counterparts, even though the expression of the HIF target genes CA9,
305 PHD3 and NDRG1 was not significantly different (Figures 6D and S6G), suggesting that cells
306 retain a memory of their hypoxic past.
307
308 In order to evaluate the hypoxic memory *in vivo* at the single cell level, we optimized our HypT
309 plasmid to include a 3' UTR for the RFP transcript (Figure S6H), in addition to the 3'UTR of the
310 GFP side, and used the 3'capture methods of chromium to analyze the scRNAseq data of MCF7-
311 HypT tumors at 4, 5, and 6 weeks. Tumor cells with detected RFP or GFP transcript were first
312 ranked based on the hypoxia signature score (Figure S6I). Since GFP positive cells could be
313 tumor cells that are in hypoxic region, or have already exited hypoxic region, the hypoxic score
314 could help distinguish the two situations. We termed the "normoxia" population based on the
315 hypoxia scores of zero or below, "hypoxia" population for the highest decile of the hypoxia
316 score, and "moderate hypoxia" for those in between. As expected, majority of the RFP positive
317 cells (dsRed) are in normoxia; GFP-hypoxia indicates cells in hypoxia, and GFP-normoxia
318 indicates cells that exited the hypoxia region (Figure 6E). The IFN/AP scores were analyzed in
319 the corresponding cell populations (Figure 6F). In all 3 time points, we observed statistically
320 significant decreased IFN/AP score in GFP-hypoxia cells compared to dsRed cells. Intriguingly,

321 from week 5 to week 6, we also observed that such decrease is maintained in the GFP-normoxia
322 cells. Therefore, these *in vivo* data supported our *in vitro* finding of hypoxic memory of IFN/AP
323 suppression.
324
325 **Erasing hypoxic memory enhances immune clearance when combined with immune**
326 **checkpoint inhibitors.**
327 To investigate the potential involvement of epigenetic regulation in the hypoxic memory of
328 IFN/AP suppression, we evaluated the ability of several epigenetic inhibitors to rescue IFN/AP
329 suppression after reoxygenation. An HDACi, MS275 (Entinostat)(56), and a low concentration
330 of a G9a/GLP inhibitor, UNC0638(57), reversed the hypoxic memory of IFN target IFIT1
331 (Figures 7A-B and S7A). To evaluate the effect *in vivo*, we performed scRNAseq analysis of the
332 NT2.5 cells in syngeneic tumors treated with vehicle, Entinostat alone, or in combination with
333 anti-CTLA4, anti-PD1, or both(58). A total of 20 tumors (4 from each group) were processed by
334 10x Chromium platform after 3 weeks of treatment, but before a significant tumor shrinkage.
335 Surprisingly, different from other luminal mouse single cell data (Figure 3B-C), decile plots of
336 the tumor cells ranked by IFN/AP score in the vehicle condition showed a positive correlation of
337 hypoxia and IFN/AP signatures, but Entinostat treatment led to a clear inverse correlation, and
338 the effect became even more obvious when combined with the immunotherapies (Figure 7C). To
339 investigate whether the existence of hypoxic memory of NT2.5 cells could potentially explain
340 this result, we performed analysis of NT2.5 cells for the long term effect of hypoxia. Indeed,
341 NT2.5 cells showed hypoxic memory of IFN target suppression after reoxygenation from both
342 4% or 1% of hypoxia exposure for 14 days (Figure 7D). It is tempted to speculate that Entinostat
343 removed the hypoxic memory and upregulated the IFN/AP signals for tumor cells in the
344 normoxic region (negative for hypoxia), leading to a clear inverse correlation of hypoxia-IFN/AP

345 scores in the scRNAseq analysis. We also found that the combination of Entinostat with
346 checkpoint blockades led to an overall increased hypoxia score in the tumors (Figure S7B),
347 suggesting more effective elimination of cells in normoxia. We further investigated the hypoxic
348 memory association with tumor growth in a syngeneic model. When NT2.5 cells grown in
349 normoxia or hypoxia (4% or 1% O_2) for 14 days were injected in immunocompetent FVB mice,
350 cells pre-cultured in 1% hypoxia generated significantly bigger tumors, compared to those pre-
351 cultured in normoxia (Figure 7E), accompanied with more immunosuppressive Arginase (Arg)+
352 granulocytic myeloid derived suppressor cells (gMDSCs) and macrophages (Figures 7F-G and
353 S7C-F). These data suggest that besides the intrinsic effect on the tumor cells, this hypoxic
354 memory can modify the recruitment of immune cells to shift the balance towards a more
355 immunosuppressive microenvironment.
356
357 **Discussion**
358 In this study, we discovered that hypoxia leads to the suppression of type I IFN signaling and
359 downstream AP pathway specifically in the luminal subtype of breast cancer cells. This effect is
360 mediated via both HIF1-dependent and HIF-independent mechanisms. Intriguingly, even after a
361 returning to normoxic conditions after a prolonged exposure to low oxygen levels, hypoxia
362 induced IFN/AP suppression can be maintained as a hypoxic memory, which is associated with
363 enhanced tumorigenesis and metastasis. This suggests a novel mechanism for the enhanced
364 metastatic capacity of tumor cells shed from hypoxic regions.
365
366 As one of the common tumor microenvironment (TME) features of solid tumors, hypoxia has
367 well-known multifaceted effects that promote tumor progression(2). Our finding on its effect in

368 suppressing tumor cell intrinsic type I IFN and AP signals provides an additional novel
369 mechanism. Type I IFN signaling has intrinsic tumor suppressive effect, by inhibiting
370 proliferation and promoting apoptosis, and it also plays a key role in immune surveillances
371 against tumors(27). Therefore, by downregulating intrinsic type I IFN as well as downstream AP
372 machinery, hypoxia provides tumor cell intrinsic and extrinsic benefits during tumor progression.
373 Of note, a study with similar topic has recently been reported(59), however with different results.
374 Whereas this report showed similar effects in all subtypes(59), we found that this hypoxia
375 mediated suppression of IFN/AP to be specific in luminal subtypes of breast cancer cells with no
376 obvious difference in basal subtype cell lines. The differences may be due to the level of hypoxia
377 used in the experiments. We mainly focused on relatively mild hypoxia condition (4%-1% O_2)
378 since this is likely to be more common across tumor types(60), while a much lower oxygen
379 levels (1%-0.1%) have been used in the other report(59). Intriguingly, we did observe differences
380 in the long term effect by different hypoxia priming, highlighting the importance in considering
381 the specific niche effects. Moreover, our scRNAseq analysis of the MMTV-PyMT tumor model
382 further supports such effect being more prominent in luminal characteristic tumor cells based on
383 the report that MMTV-PyMT model progresses with a loss of luminal features over time(39).
384 scRNAseq analysis of other syngeneic breast cancer models also showed a clear inverse
385 correlation of hypoxia and IFN/AP scores in tumor cells sorted based on Cd24 surface marker
386 likely enriching luminal type of tumor cells(40). However, the exact mechanisms underlying the
387 luminal versus basal subtypes in terms of their hypoxic responses are not yet clear and warrants
388 further investigation, which may contribute to a better understanding of why luminal tumors are
389 immune “colder” tumors than the basal subtypes.
390

391 We also found that hypoxia downregulates IFN/AP signal in both HIF-dependent and -
392 independent manners. An intriguing novel finding is the distinct effect of HIF1α and HIF2α in
393 regulating ISG expression, with HIF1α suppressing whereas HIF2α inducing ISG genes, which
394 may add another layer of heterogeneity pending on the level of HIF1α and HIF2α in a particular
395 cell. Although we have attempted to elucidate the HIF-independent mechanism, the exact
396 regulation is unclear and worth of further investigation. Different from previously mentioned
397 mechanism in which mitochondrial dsRNA quantity is reduced in hypoxia compared to
398 normoxia(41), we did not detect significant differences in the mitochondrial dsRNA levels.
399 Epigenetic factors may play an indirect role since we observed changes in global histone
400 methylations in hypoxia. Epigenetic mechanisms indeed contribute to hypoxic memory
401 maintenances.
402
403 Our intriguing finding of hypoxic memory of IFN/AP suppression is, to the best of our
404 knowledge, the first reported long term suppression of such signal. During our manuscript
405 preparation, a study has utilized a similar 2-plasmid Cre-loxP mediated hypoxia tracing system
406 to evaluate the long-term effect of hypoxia *in vivo*(34). The study noted a long-term effect of
407 hypoxia that promotes metastasis, but only utilized the basal subtype of breast cancer cells. In
408 that context, the hypoxic memory mainly persists via upregulated genes that promote cell
409 survival in the presence of high levels of ROS. As we have shown that hypoxia-mediated
410 IFN/AP suppression is prominent in luminal subtype, it is likely that the signals lasting longer as
411 hypoxic memory is subtype dependent and mechanisms could be heterogeneous. A surprising
412 finding is that mild (4% O_2) and long term (14 days) of hypoxia exposure, but not severe (1%
413 O_2), nor a short exposure (3 days), lead to the prolonged memory of IFN/AP suppression in

414 MCF7 cells. While in NT2.5 cells, hypoxic memory can be established by both mild and severe
415 hypoxia conditions. The unique hypoxia priming condition suggests specific molecular
416 mechanisms are involved in establishing and/or maintaining such cellular memory in a cell type
417 dependent manner, which warrants further analysis.
418
419 Within solid tumors, hypoxic features constantly change due to tumor growth and cellular
420 movement. Hypoxic memory of IFN/AP suppression could contribute to immune evasion and
421 reduce efficacy of checkpoint immunotherapies. As shown in our *in vitro* MCF7 data and *in vivo*
422 data of NT2.5 syngeneic tumors, Entinostat upregulates IFN/AP signals of cells in normoxic
423 regions, resulting in increased hypoxia scores when combined with immunocheckpoint
424 treatment. Despite the limitation of one static time point and the correlative nature, the data
425 suggests the possibility that for NT2.5 cells with hypoxic memory (ie. low IFN/AP score in the
426 normoxia region) in vehicle condition, such memory can be "erased" by Entinostat treatment
427 thereby leading to improved immune clearance of cells in normoxic area by the immune
428 checkpoint therapies. A more direct link with multiple time points will be worth evaluating in
429 future studies. Moreover, our data of the syngeneic model showed that NT2.5 cells pre-
430 conditioned in hypoxia lead to bigger tumor formation, with recruitment of more
431 immunosuppressive cell types in the TME. Furthermore, the prolonged suppression of IFN/AP
432 would likely also contribute to the immune evasive feature commonly seen in CTCs. Indeed,
433 after exposure to hypoxia, only those CTCs with the capacity for a hypoxic memory of IFN/AP
434 suppression showed enhanced tumorigenesis and metastasis. Our study suggests a novel concept
435 of hypoxia induced long term cellular memory as a potential mechanism for promoting tumor
436 progression.

437

438 **References**

439 1. Bertout JA, Patel SA, Simon MC. The impact of O 2 availability on human cancer. Nat Rev
440 Cancer. Nature Publishing Group; 2008;8:967–75.

441 2. Rankin EB, Nam J-M, Giaccia AJ. Hypoxia: Signaling the Metastatic Cascade. Trends
442 Cancer. 2016;2:295–304.

443 3. Pugh CW, Ratcliffe PJ. Regulation of angiogenesis by hypoxia: role of the HIF system. Nat
444 Med. Nature Publishing Group; 2003;9:677–84.

445 4. Eisinger-Mathason TSK, Zhang M, Qiu Q, Skuli N, Nakazawa MS, Karakasheva T, et al.
446 Hypoxia-Dependent Modification of Collagen Networks Promotes Sarcoma Metastasis.
447 Cancer Discov. American Association for Cancer Research; 2013;3:1190–205.

448 5. Yang M-H, Wu M-Z, Chiou S-H, Chen P-M, Chang S-Y, Liu C-J, et al. Direct regulation of
449 TWIST by HIF-1α promotes metastasis. Nat Cell Biol. Nature Publishing Group;
450 2008;10:295–305.

451 6. Li Z, Bao S, Wu Q, Wang H, Eyler C, Sathornsumetee S, et al. Hypoxia-Inducible Factors
452 Regulate Tumorigenic Capacity of Glioma Stem Cells. Cancer Cell. Elsevier; 2009;15:501–
453 13.

454 7. Iriondo O, Rábano M, Domenici G, Carlevaris O, López-Ruiz JA, Zabalza I, et al. Distinct
455 breast cancer stem/progenitor cell populations require either HIF1α or loss of PHD3 to
456 expand under hypoxic conditions. Oncotarget. 2015;6:31721–39.

457 8. Erler JT, Bennewith KL, Cox TR, Lang G, Bird D, Koong A, et al. Hypoxia-Induced Lysyl
458 Oxidase Is a Critical Mediator of Bone Marrow Cell Recruitment to Form the Premetastatic
459 Niche. Cancer Cell. Elsevier; 2009;15:35–44.

460 9. Wong CC-L, Gilkes DM, Zhang H, Chen J, Wei H, Chaturvedi P, et al. Hypoxia-inducible
461 factor 1 is a master regulator of breast cancer metastatic niche formation. Proc Natl Acad
462 Sci. National Academy of Sciences; 2011;108:16369–74.

463 10. Bruick RK, McKnight SL. A Conserved Family of Prolyl-4-Hydroxylases That Modify HIF.
464 Science. American Association for the Advancement of Science; 2001;294:1337–40.

465 11. Huang LE, Gu J, Schau M, Bunn HF. Regulation of hypoxia-inducible factor 1α is mediated
466 by an O2-dependent degradation domain via the ubiquitin-proteasome pathway. Proc Natl
467 Acad Sci. National Academy of Sciences; 1998;95:7987–92.

468 12. Ivan M, Kondo K, Yang H, Kim W, Valiando J, Ohh M, et al. HIFα Targeted for VHL-
469 Mediated Destruction by Proline Hydroxylation: Implications for O2 Sensing. Science.
470 American Association for the Advancement of Science; 2001;292:464–8.

471 13. Semenza GL. Hypoxia-Inducible Factors in Physiology and Medicine. Cell. Elsevier;
472 2012;148:399–408.

473 14. Kaelin WG, Ratcliffe PJ. Oxygen Sensing by Metazoans: The Central Role of the HIF
474 Hydroxylase Pathway. Mol Cell. Elsevier; 2008;30:393–402.

475 15. Ivan M, Kaelin WG. The EGLN-HIF O 2 -Sensing System: Multiple Inputs and Feedbacks.
476 Mol Cell. 2017;66:772–9.

477 16. Thienpont B, Steinbacher J, Zhao H, D'Anna F, Kuchnio A, Ploumakis A, et al. Tumour
478 hypoxia causes DNA hypermethylation by reducing TET activity. Nature. 2016;537:63.

479 17. Batie M, Frost J, Frost M, Wilson JW, Schofield P, Rocha S. Hypoxia induces rapid changes
480 to histone methylation and reprograms chromatin. Science. American Association for the
481 Advancement of Science; 2019;363:1222–6.

482 18. Chakraborty AA, Laukka T, Myllykoski M, Ringel AE, Booker MA, Tolstorukov MY, et al.
483 Histone demethylase KDM6A directly senses oxygen to control chromatin and cell fate.
484 Science. American Association for the Advancement of Science; 2019;363:1217–22.

485 19. Choudhry H, Harris AL. Advances in Hypoxia-Inducible Factor Biology. Cell Metab
486 [Internet]. 2017 [cited 2017 Dec 4]; Available from:
487 http://www.sciencedirect.com/science/article/pii/S1550413117306174

488 20. Chouaib S, Noman MZ, Kosmatopoulos K, Curran MA. Hypoxic stress: obstacles and
489 opportunities for innovative immunotherapy of cancer. Oncogene. Nature Publishing
490 Group; 2017;36:439–45.

491 21. Vito A, El-Sayes N, Mossman K. Hypoxia-Driven Immune Escape in the Tumor
492 Microenvironment. Cells. Multidisciplinary Digital Publishing Institute; 2020;9:992.

493 22. Movahedi K, Laoui D, Gysemans C, Baeten M, Stangé G, Bossche JV den, et al. Different
494 Tumor Microenvironments Contain Functionally Distinct Subsets of Macrophages Derived
495 from Ly6C(high) Monocytes. Cancer Res. American Association for Cancer Research;
496 2010;70:5728–39.

497 23. Van Overmeire E, Laoui D, Keirsse J, Van Ginderachter JA, Sarukhan A. Mechanisms
498 Driving Macrophage Diversity and Specialization in Distinct Tumor Microenvironments
499 and Parallelisms with Other Tissues. Front Immunol [Internet]. Frontiers; 2014 [cited 2021
500 May 28];5. Available from:
501 https://www.frontiersin.org/articles/10.3389/fimmu.2014.00127/full

502 24. Chiu DK-C, Tse AP-W, Xu IM-J, Di Cui J, Lai RK-H, Li LL, et al. Hypoxia inducible factor
503 HIF-1 promotes myeloid-derived suppressor cells accumulation through ENTPD2/CD39L1
504 in hepatocellular carcinoma. Nat Commun. Nature Publishing Group; 2017;8:517.

505 25. Hatfield SM, Kjaergaard J, Lukashev D, Schreiber TH, Belikoff B, Abbott R, et al.
506 Immunological mechanisms of the antitumor effects of supplemental oxygenation. Sci
507 Transl Med. American Association for the Advancement of Science; 2015;7:277ra30-
508 277ra30.

509 26. Fischer K, Hoffmann P, Voelkl S, Meidenbauer N, Ammer J, Edinger M, et al. Inhibitory
510 effect of tumor cell–derived lactic acid on human T cells. Blood. 2007;109:3812–9.

511 27. Snell LM, McGaha TL, Brooks DG. Type I Interferon in Chronic Virus Infection and
512 Cancer. Trends Immunol. Elsevier; 2017;38:542–57.

513 28. Boukhaled GM, Harding S, Brooks DG. Opposing Roles of Type I Interferons in Cancer
514 Immunity. Annu Rev Pathol Mech Dis. Annual Reviews; 2021;16:167–98.

515 29. Parker BS, Rautela J, Hertzog PJ. Antitumour actions of interferons: implications for cancer
516 therapy. Nat Rev Cancer. Nature Publishing Group; 2016;16:131–44.

517 30. Yu M, Bardia A, Wittner BS, Stott SL, Smas ME, Ting DT, et al. Circulating breast tumor
518 cells exhibit dynamic changes in epithelial and mesenchymal composition. Science.
519 2013;339:580–4.

520 31. Yu M, Bardia A, Aceto N, Bersani F, Madden MW, Donaldson MC, et al. Ex vivo culture of
521 circulating breast tumor cells for individualized testing of drug susceptibility. Science.
522 2014;345:216–20.

523 32. Klotz R, Thomas A, Teng T, Han SM, Iriondo O, Li L, et al. Circulating Tumor Cells
524 Exhibit Metastatic Tropism and Reveal Brain Metastasis Drivers. Cancer Discov.
525 2020;10:86–103.

526 33. Donato C, Kunz L, Castro-Giner F, Paasinen-Sohns A, Strittmatter K, Szczerba BM, et al.
527 Hypoxia Triggers the Intravasation of Clustered Circulating Tumor Cells. Cell Rep
528 [Internet]. Elsevier; 2020 [cited 2020 Sep 23];32. Available from:
529 https://www.cell.com/cell-reports/abstract/S2211-1247(20)31094-9

530 34. Godet I, Shin YJ, Ju JA, Ye IC, Wang G, Gilkes DM. Fate-mapping post-hypoxic tumor
531 cells reveals a ROS-resistant phenotype that promotes metastasis. Nat Commun. Nature
532 Publishing Group; 2019;10:4862.

533 35. Aguilera TA, Rafat M, Castellini L, Shehade H, Kariolis MS, Hui AB-Y, et al.
534 Reprogramming the immunological microenvironment through radiation and targeting Axl.
535 Nat Commun. 2016;7:13898.

536 36. Song H, Shahverdi K, Huso DL, Wang Y, Fox JJ, Hobbs RF, et al. An Immunotolerant
537 HER-2/neu Transgenic Mouse Model of Metastatic Breast Cancer. Clin Cancer Res.
538 American Association for Cancer Research; 2008;14:6116–24.

539 37. Buffa FM, Harris AL, West CM, Miller CJ. Large meta-analysis of multiple cancers reveals
540 a common, compact and highly prognostic hypoxia metagene. Br J Cancer. Nature
541 Publishing Group; 2010;102:428–35.

542 38. Kuchnio A, Moens S, Bruning U, Kuchnio K, Cruys B, Thienpont B, et al. The Cancer Cell
543 Oxygen Sensor PHD2 Promotes Metastasis via Activation of Cancer-Associated
544 Fibroblasts. Cell Rep. 2015;12:992–1005.

545 39. Lin EY, Jones JG, Li P, Zhu L, Whitney KD, Muller WJ, et al. Progression to Malignancy in
546 the Polyoma Middle T Oncoprotein Mouse Breast Cancer Model Provides a Reliable Model
547 for Human Diseases. Am J Pathol. 2003;163:2113–26.

548 40. Yeo SK, Zhu X, Okamoto T, Hao M, Wang C, Lu P, et al. Single-cell RNA-sequencing
549 reveals distinct patterns of cell state heterogeneity in mouse models of breast cancer. Zwart
550 W, Murphy ME, Zwart W, Magnani L, Natrajan R, editors. eLife. eLife Sciences
551 Publications, Ltd; 2020;9:e58810.

552 41. Arnaiz E, Miar A, Dias AG, Prasad N, Schulze U, Waithe D, et al. Hypoxia regulates
553 endogenous double-stranded RNA production via reduced mitochondrial DNA
554 transcription. bioRxiv. Cold Spring Harbor Laboratory; 2020;2020.07.31.230300.

555 42. Yu M, Levine SJ. Toll-like receptor 3, RIG-I-like receptors and the NLRP3 inflammasome:
556 Key modulators of innate immune responses to double-stranded RNA viruses. Cytokine
557 Growth Factor Rev. 2011;22:63–72.

558 43. Semenza GL. Hypoxia-Inducible Factors in Physiology and Medicine. Cell. 2012;148:399–
559 408.

560 44. Wang Q, Li L-H, Gao G-D, Wang G, Qu L, Li J-G, et al. HIF-1α up-regulates NDRG1
561 expression through binding to NDRG1 promoter, leading to proliferation of lung cancer
562 A549 cells. Mol Biol Rep. 2013;40:3723–9.

563 45. Strowitzki MJ, Cummins EP, Taylor CT. Protein Hydroxylation by Hypoxia-Inducible
564 Factor (HIF) Hydroxylases: Unique or Ubiquitous? Cells. 2019;8:384.

565 46. Provenzano R, Besarab A, Sun CH, Diamond SA, Durham JH, Cangiano JL, et al. Oral
566 Hypoxia–Inducible Factor Prolyl Hydroxylase Inhibitor Roxadustat (FG-4592) for the
567 Treatment of Anemia in Patients with CKD. Clin J Am Soc Nephrol CJASN. 2016;11:982–
568 91.

569 47. Tian Y-M, Yeoh KK, Lee MK, Eriksson T, Kessler BM, Kramer HB, et al. Differential
570 Sensitivity of Hypoxia Inducible Factor Hydroxylation Sites to Hypoxia and Hydroxylase
571 Inhibitors. J Biol Chem. 2011;286:13041–51.

572 48. Yan Q, Bartz S, Mao M, Li L, Kaelin WG. The Hypoxia-Inducible Factor 2 α N-Terminal
573 and C-Terminal Transactivation Domains Cooperate To Promote Renal Tumorigenesis In
574 Vivo. Mol Cell Biol. 2007;27:2092–102.

575 49. Batie M, Frost J, Frost M, Wilson JW, Schofield P, Rocha S. Hypoxia induces rapid changes
576 to histone methylation and reprograms chromatin. Science. 2019;363:1222–6.

577 50. Heinemann B, Nielsen JM, Hudlebusch HR, Lees MJ, Larsen DV, Boesen T, et al. Inhibition
578 of demethylases by GSK-J1/J4. Nature. 2014;514:E1–2.

579 51. Tumber A, Nuzzi A, Hookway ES, Hatch SB, Velupillai S, Johansson C, et al. Potent and
580 Selective KDM5 Inhibitor Stops Cellular Demethylation of H3K4me3 at Transcription Start
581 Sites and Proliferation of MM1S Myeloma Cells. Cell Chem Biol. 2017;24:371–80.

582 52. Chu C-H, Wang L-Y, Hsu K-C, Chen C-C, Cheng H-H, Wang S-M, et al. KDM4B as a
583 Target for Prostate Cancer: Structural Analysis and Selective Inhibition by a Novel
584 Inhibitor. J Med Chem. American Chemical Society; 2014;57:5975–85.

585 53. Gaughan L, Stockley J, Coffey K, O'Neill D, Jones DL, Wade M, et al. KDM4B is a Master
586 Regulator of the Estrogen Receptor Signalling Cascade. Nucleic Acids Res. Oxford
587 Academic; 2013;41:6892–904.

588 54. Shi L, Sun L, Li Q, Liang J, Yu W, Yi X, et al. Histone demethylase JMJD2B coordinates
589 H3K4/H3K9 methylation and promotes hormonally responsive breast carcinogenesis. Proc
590 Natl Acad Sci. National Academy of Sciences; 2011;108:7541–6.

591 55. Varia MA, Calkins-Adams DP, Rinker LH, Kennedy AS, Novotny DB, Fowler WC, et al.
592 Pimonidazole: A Novel Hypoxia Marker for Complementary Study of Tumor Hypoxia and
593 Cell Proliferation in Cervical Carcinoma. Gynecol Oncol. 1998;71:270–7.

594 56. Saito A, Yamashita T, Mariko Y, Nosaka Y, Tsuchiya K, Ando T, et al. A synthetic inhibitor
595 of histone deacetylase, MS-27-275, with marked in vivo antitumor activity against human
596 tumors. Proc Natl Acad Sci. National Academy of Sciences; 1999;96:4592–7.

597 57. Vedadi M, Barsyte-Lovejoy D, Liu F, Rival-Gervier S, Allali-Hassani A, Labrie V, et al. A
598 chemical probe selectively inhibits G9a and GLP methyltransferase activity in cells. Nat
599 Chem Biol. 2011;7:566–74.

600 58. Christmas BJ, Rafie CI, Hopkins AC, Scott BA, Ma HS, Cruz KA, et al. Entinostat Converts
601 Immune-Resistant Breast and Pancreatic Cancers into Checkpoint-Responsive Tumors by
602 Reprogramming Tumor-Infiltrating MDSCs. Cancer Immunol Res. American Association
603 for Cancer Research; 2018;6:1561–77.

604 59. Miar A, Arnaiz E, Bridges E, Beedie S, Cribbs AP, Downes DJ, et al. Hypoxia Induces
605 Transcriptional and Translational Downregulation of the Type I IFN Pathway in Multiple
606 Cancer Cell Types. Cancer Res. American Association for Cancer Research;
607 2020;80:5245–56.

608 60. Muz B, de la Puente P, Azab F, Azab AK. The role of hypoxia in cancer progression,
609 angiogenesis, metastasis, and resistance to therapy. Hypoxia. 2015;3:83–92.

610 61. Nguyen-Ngoc K-V, Shamir ER, Huebner RJ, Beck JN, Cheung KJ, Ewald AJ. 3D Culture
611 Assays of Murine Mammary Branching Morphogenesis and Epithelial Invasion. In: Nelson
612 CM, editor. Tissue Morphog [Internet]. New York, NY: Springer New York; 2015 [cited
613 2023 Jul 9]. page 135–62. Available from: https://link.springer.com/10.1007/978-1-4939-
614 1164-6_10

615 62. Harada H, Inoue M, Itasaka S, Hirota K, Morinibu A, Shinomiya K, et al. Cancer cells that
616 survive radiation therapy acquire HIF-1 activity and translocate towards tumour blood
617 vessels. Nat Commun. 2012;3:783.

618 63. Satija R, Farrell JA, Gennert D, Schier AF, Regev A. Spatial reconstruction of single-cell
619 gene expression data. Nat Biotechnol. 2015;33:495–502.

620 64. Babraham Bioinformatics - Trim Galore! [Internet]. [cited 2021 Oct 11]. Available from:
621 https://www.bioinformatics.babraham.ac.uk/projects/trim_galore/

622 65. Dobin A, Davis CA, Schlesinger F, Drenkow J, Zaleski C, Jha S, et al. STAR: ultrafast
623 universal RNA-seq aligner. Bioinforma Oxf Engl. 2013;29:15–21.

624 66. Anders S, Pyl PT, Huber W. HTSeq--a Python framework to work with high-throughput
625 sequencing data. Bioinforma Oxf Engl. 2015;31:166–9.

626 67. Love MI, Huber W, Anders S. Moderated estimation of fold change and dispersion for
627 RNA-seq data with DESeq2. Genome Biol. 2014;15:550.

628 68. Ritchie ME, Phipson B, Wu D, Hu Y, Law CW, Shi W, et al. limma powers differential
629 expression analyses for RNA-sequencing and microarray studies. Nucleic Acids Res.
630 2015;43:e47.

631 69. Subramanian A, Tamayo P, Mootha VK, Mukherjee S, Ebert BL, Gillette MA, et al. Gene
632 set enrichment analysis: a knowledge-based approach for interpreting genome-wide
633 expression profiles. Proc Natl Acad Sci U S A. 2005;102:15545–50.

634 70. Mootha VK, Lindgren CM, Eriksson K-F, Subramanian A, Sihag S, Lehar J, et al. PGC-
635 1alpha-responsive genes involved in oxidative phosphorylation are coordinately
636 downregulated in human diabetes. Nat Genet. 2003;34:267–73.

637 71. Aguilera TA, Elghonaimy EA, Shehade H, Rafat M, Castellini L, Jiang D, et al. Induced
638 Tumor Heterogeneity Reveals Factors Informing Radiation and Immunotherapy
639 Combinations. Clin Cancer Res. American Association for Cancer Research;
640 2020;26:2972–85.

641

642 **Acknowledgements.** We thank the USC Flow Cytometry Facility and USC Molecular Genomics
643 Core for their technical support; D. Ruble and members of CHLA Molecular Pathology
644 Genomics Core for technical assistance; Drs. J. Lang and T. Aguilera for providing cell lines;
645 Drs. Q. Zhang and H. Harada for providing reagents; C. Lytal for editing the manuscript. This
646 research was supported by the following: The National Institutes of Health (NIH) grant DP2
647 CA206653 (M.Y.), the Stop Cancer Foundation (M.Y.), the PEW Charitable Trusts and the
648 Alexander & Margaret Stewart Trust (M.Y.), the Department of Defense Era of Hope Scholar
649 Award (M.Y.), the Richard Merkin Foundation (M.Y.), the Broad Fellowship (O.I.), and the NIH
650 grant T90DE021982 (trainees D.M. and Y.A.). The project described was supported in part (core
651 facilities) by award number P30CA014089 from the National Cancer Institute. This research was
652 also supported by funds through the Maryland Department of Heath's Cigarette Restitution Fund
653 Program (CH-649-CRF).
654
655 **Author Contributions.** O.I. and M.Y. conceived the study. O.I., D.M., Y.L. and M.Y. designed
656 experiments. O.I., D.M., Y.L., A.D., G.L., S.H. and M.Y. performed experiments. O.I., D.M.,
657 Y.L., C.R.C., A.T., Y.A., V.O., M.M., A.D., G.L., B.A.B., E.R.T. and M.Y. contributed to
658 analysis and interpretation of data. C.R.C., A.T., Y.A., M.M., A.S. and C.M. conducted
659 computational analyses. E.R.T. provided scRNAseq data of syngeneic tumors. O.I. and M.Y.
660 wrote the manuscript. All authors edited and commented on the manuscript. M.Y. supervised the
661 study.
662
663

664 **Methods**

665

666 **Cell culture and reagents**

667 CTC lines derived from patients with luminal breast tumors(31) were cultured in ultra-low
668 attachment plates (Corning) with RPMI 1640 supplemented with 20 ng/ml EGF, 20 ng/ml bFGF,
669 1X B27 and 1X antibiotic/antimycotic. CTCs were maintained in a Nuaire NU-5831 incubator at
670 4% O_2 and 5% CO_2, and media was changed every 3 or 4 days. For normoxia vs hypoxia
671 experiments, equal number of cells were plated and kept in normoxia or hypoxia (4% O_2)
672 conditions for the indicated duration.

673

674 MCF7, MDA-MB-231, HS578T and HEK293T cells were purchased from the American Type
675 Culture Collection and were maintained in DMEM supplemented with 10% FBS. T47D and
676 BT474 cells were provided by Dr. Julie Lang and were cultured in RPMI media with 10% FBS.
677 Py117 and PY8119 cells were provided by Dr. Todd Aguilera and maintained in F12 media
678 containing 5% fetal clone II (Hyclone) and MITO+ (1:1000 dilution, Corning). NT2.5 cells were
679 provided by Dr. Evanthia Roussos Torres and cultured in RPMI media supplemented with 20%
680 FBS, 1.2% Hepes, 1% L-Glutamine, 1% non-essential aminoacids, 1% sodium pyruvate and
681 0.2% insulin. For normoxia vs hypoxia experiments, cells were moved to hypoxic incubators
682 (Nuaire NU-5831 for 4% O_2, Biospherix ProOx C21 for 1% O_2) 7-8 hours after plating, to ensure
683 that cells had adhered to dish by the time hypoxia treatment started. For the 14-day-long
684 treatments, cells were split every 3 or 4 days and put back in hypoxia once they adhered to the
685 dish. For experiments with small molecule inhibitors, MCF7 or T47D cells were plated, and once
686 cells adhered to the plates, inhibitors were added in fresh media. Inhibitor concentrations and the

687 duration of the treatments are specified in the figure legends. The inhibitors used in this study
688 were FG-4592 (Selleckchem, S1007), GSK-J4 (Selleckchem, S7070), KDM5-C70 (Xcess
689 Biosciences, M60192-2), NSC636819 (Sigma, 5131996), MS275 (Selleckchem, S1053) and
690 UNC0638 (U4885).
691
692 All cultures were routinely (every 1-2 months) tested for mycoplasma contamination using
693 MycoAlert (Lonza). Autosomal STR profiles for cell line authentication were performed by the
694 University of Arizona Genetics Core.
695
696
697 **3D culture**
698 MCF7-HypT cells were FACS sorted for $RFP^{+}GFP^{-}$ phenotype. Cells were counted and 20,000
699 cells were plated in each well of a 24-well ultra-low attachment plate to allow cells to form small
700 aggregates. The following day, Matrigel-collagen mixture was prepared and MCF7-HypT cells
701 were plated into 8-chamber slides (Corning, 354118) following protocol by Nguyen-Ngoc et al
702 (61). Images of spheres were taken the day of plating and every 2-3 days to track the conversion
703 of RFP^{+} cells to GFP^{+} cells over time. Images were taken on a Keyence BZ-9000 fluorescence
704 microscope.
705
706 **Generation of stable cell lines**
707
708 PHAGE2-EF1α-LoxP-DsRED-STOP-LoxP-eGFP (Addgene, 62732) and pLKO.1-5xHRE-
709 CRE-ODD plasmids were used for producing MCF7-HypT cells. To modify the CRE reporter,

710 the bGH poly(A) signal was inserted into the NheI site, downstream of DsRed. The bGH poly(A)
711 signal was PCR amplified from pX459 (Addgene, 62988) using primers forward, 5'-
712 AAGTCTAGACGCTCCCCAGCATGCCTGCT-3' and reverse, 5'-
713 AGGGCTAGCCGACTGTGCCTTCTAGTTGCCAGCCA-3'. To generate the pLKO-5xHRE-
714 CRE-ODD plasmid, pLKO.1-neo (Addgene, 13425) was used as the backbone. The U6 promoter
715 was deleted and replaced with an XbaI site using NEB Q5 site directed mutagenesis kit (NEB
716 Cat# E0554S) with primers forward, 5'-AAAAATCTAGATGTGGAAAGGACGAAACACC-
717 3'; reverse, 5'- AAAAATCTAGAGAAATAGGCCCTCGGTGAAG-3' according to
718 manufacturer's protocol. The reaction was transformed into chemically competent NEB Stable
719 cells (NEB Cat#C3040H) and the plasmid was verified by restriction enzyme digestion and
720 Sanger sequencing. Subsequent cloning steps were performed to generate pLKO-5xHRE-CRE-
721 ODD by using primers forward, 5'-
722 AAAAAACTAGTGCTAGCGGTAGGCGTGTACGGTGGGAGGTCTATATAAGCAGAGCT
723 C – 3', reverse 5'-
724 AAAAATCTAGAGATCTGACGGTTCACTAAACGAGCTCTGCTTATATAGACC – 3';
725 forward, 5'- AAAAAGCTAGCTCTAGAACCATGGCCAATTTACTGACCGTACACC-3',
726 reverse, 5'- AAAAAGCTAGCGGCAACTAGAAGGCACAGTCG – 3'; forward, 5'-
727 AAAAAGCTAGCGGTGGAGAGAGAGACAGAGACAG -3', reverse, 5'-
728 AAAAAGCTAGCGGTGGATCCTGCAAAAAGAACAAGTAGC -3', along with the pEF-
729 5xHRE-GFP (Addgene, 46926) and pEF-5xHRE-CRE-ER^{T2}-ODD-myc(62) plasmids as
730 templates. For HIF mutant cell lines, we made retrovirus using HA-HIF1α P402A/P564A-
731 pBabe-puro (Addgene, 19005) and HA-HIF2α P405A/P531A/N847Q-pBabe-puro (Addgene,
732 19006). To generate lentivirus for HIF mutants we subcloned HIF1α mutant from HA-HIF1α

733 P402A/P564A-pcDNA3 (Addgene, 18955) into pCDH-CMV (Addgene, 72265) using BamHI
734 and NotI restriction sites and HIF2α mutant from the pBabe retroviral vector into pCDH-CMV
735 using BamHI and SalI sites.
736
737 Lentiviral particles were produced by co-transfecting 293T cells with lentiviral expression
738 vectors in combination with second generation (VSV-G and pCMV-dR.8.91, for pLKO-5xHRE-
739 CRE-ODD, Lenti-dCas9-KRAB-Blast and sgRNA plasmids) or third generation (VSV-G,
740 PMDL and REV, for PHAGE2-EF1α-LoxP-DsRED-STOP-LoxP-eGFP) lentivirus packaging
741 plasmids, using the TransitLT1 transfection reagent (Mirus). Viruses were concentrated with
742 lenti-X concentrator (Clontech). Cell lines to be infected with virus were seeded with 200,000
743 cells in each well of a 6-well plate. The following day, polybrene (8μg/ml) and concentrated
744 virus were added to each well and incubated overnight. Cells were then selected for infection
745 using puromycin (1 μg/ml), geneticin (0.5 mg/ml) or FACS sorting.
746
747 For CRISPR-knockout (KO), guide RNA sequences were cloned into pX458 (Addgene, 48138).
748 sgRNA sequences for ARNT were obtained from previously published paper (Chakraborty et al.,
749 2019): sgRNA1 ARNT, 5'-CACCGGGCTATTAAGCGACGGTCA-3', 5'-
750 AAACTGACCGTCGCTTAATAGCCC-3'; sgRNA2 ARNT, 5'-
751 CACCGAGAAACGGCCATGCGTAAGA-3', 5'-AAACTCTTACGCATGGCCGTTTCTC-3'.
752 Plasmids were transiently transfected into MCF7 cells using Lipofectamine 3000 according to
753 the manufacturer's protocol (ThermoFisher, L3000015). After three days, GFP+ cells were
754 sorted into individual wells for clonal analysis. Alt-R® Genome Editing Detection Kit (IDT

755 Cat#1075932) was used to screen clones for edited genomes within the targeted region and then
756 validated by western blot for gene knockout.
757
758 **Mouse tumor assays**
759 The animal protocol was approved by the Institutional Animal Care and Use Committee of the
760 University of Southern California. For orthotopic injections, 6 to 8 weeks-old female NSG mice
761 (Jackson Laboratory) were anesthetized with isofluorane and GFP-Luc labelled cells or MCF7-
762 HypT cells resuspended in 1:1 PBS and Matrigel (BD Biosciences) were injected into the fourth
763 mammary fat pad. Tumor growth was evaluated by *in vivo* imaging or by measuring the tumor
764 size with a caliper. Tumor volume was calculated using the formula $V = \pi \times [d^2 \times D] / 6$, were d
765 and D are the minor and major tumor axes respectively. For tail vein injection, 100,000 GFP-Luc
766 expressing cells were injected into the lateral tail vein of 6 to 8 weeks old female NSG mice.
767 Signals from luciferase-tagged cells were monitored biweekly. Mice were imaged using IVIS
768 Lumina II (Perkin Elmer) following intraperitoneal injection of 150 µl of D-Luciferin substrate at
769 30 mg/ml (Sid Labs). In all cases, mice were supplemented with 0.36 mg 90-day slow release
770 17β-Estradiol pellets (Innovative Research of America, Cat# NE-121). For tumor formation
771 experiments with NT2.5 cells, 6 to 8 weeks-old female FVB mice (Jackson Laboratory) were
772 used and tumor cells ($1x10^6$) were resuspended in PBS and injected into the fourth mammary fat
773 pad. For full methods describing derivation of NT2.5 tumors used for scRNAseq please see(58).
774
775 **Tumor dissociation**
776 Tumors were dissected and collected in cold PBS. A piece of tumor was saved for fixation and
777 immunostaining when needed. Tumors were minced and placed in dissociation media consisting

778 of RPMI supplemented with 2 mg/ml collagenase I, 5% FBS and 15 U/ml DNAse. Samples were
779 dissociated using the gentleMACS dissociator (Miltenyi Biotec), and filtered through a 70 µm
780 cell strainer. After red blood cell lysis, cell suspensions were washed and used as described
781 below.
782
783 **Flow cytometry and cell sorting**
784 For immune cells analysis of NT2.5 tumors, dissociated cell suspensions were cryopreserved
785 with 90% FBS and 10% DMSO. Once thawed, $5X10^6$ cells per mL were washed with cold PBS
786 and blocked in PBS with Rat Anti-Mouse CD16/CD32 (Mouse BD Fc Block™, BD
787 Biosciences) for 15 min at 4ºC in the dark. Then, staining of cell surface markers for myeloid
788 cell phenotyping was performed by incubating cells with fluorescent-labeled primary antibodies
789 for 30 min at 4 ºC in the dark. Cells were then fixed and permeabilized using Cyto-Fast™
790 Fix/Perm Buffer Set (Biolegend) before intracellular staining of Arginase I. LIVE/DEAD™
791 Fixable Aqua Dead Cell Stain Kit (ThermoFisher) was used as a viability marker. Antibodies
792 used were CD86 (Biolegend, 105037), F4/80 (Biolegend 123141), MHCII (BD Biosciences
793 562009), Ly6C (Biolegend, 128012), CD11b (Biolegend, 101207), CD206 (Biolegend, 141732),
794 Ly6G (BD Biosciences, 560599), CD11c (BD Biosciences, 560583), CD3 (BD Biosciences,
795 560590) and Arginase 1 (Thermo Fisher 48-3697-82). For MHC-I analysis, BRx68 cells grown
796 in different conditions were stained with HLA-ABC antibody (Biolegend, 311410). The
797 myeloid-derived suppressor cells (MDSC) were gated by $CD3^-/CD11^+/MHCII^-$ and macrophages
798 were gated by $CD3^-/MHCII^+/F4/80^+$. The granulocytic MDSCs (gMDSCs) were identified as
799 $Ly6G^+/Ly6C^{int}$ MDSCs and myeloid MDSCs (mMDSCs) were identified as $Ly6G^{low}/Ly6C^+$
800 MDSC. The Attune NxT cyometer (Thermo Fisher Scientific) was used for these analyses.

801

802 For FACS sorting, cell suspensions from MCF7-HypT tumors were washed with PBS, blocked
803 in PBS with 10% FBS and 1 µg/ml mouse Fc Block (BD Biosciences) for 15 minutes and
804 incubated with the human-specific anti-CD298-APC antibody (Biolegend, 341706) for 30
805 minutes. DAPI (1 µg/ml) was used as a viability marker. $CD298^{+}DAPI^{-}GFP^{+}RFP^{-}$ and
806 $CD298^{+}DAPI^{-}GFP^{-}RFP^{+}$ cells were sorted into pre-chilled tubes with PBS, centrifuged and lysed
807 with Quick RNA lysis buffer to proceed with RNA extraction. For sorting RFP+ cells from
808 MCF7-HypT cells grown *in vitro*, cells were collected, resuspended in cold 1% BSA in PBS
809 with DAPI (1 µg/ml), and sorted. FACS Aria II (BD Biosciences) was used for cell sorting.
810

811 **Single cell library preparation and data processing**

812 The Chromium™ Single Cell Reagent Kit v2 or Next GEM Multiome kit (10x Genomics) were
813 used for single cell RNAseq (Figure S2) or ATAC and gene expression (Figure 6E-F)
814 respectively. On the day of scRNAseq processing, tumors from 12- and 16-week-old mice were
815 dissociated as previously described. After washes with cold PBS with 0.04% BSA, 6000 cells
816 were loaded into a Single Cell A Chip. Tumors processed with Next GEM Multiome kit were
817 fresh frozen prior nuclei isolation. Nuclei isolation and permeabilization was performed
818 following 10x Genomics' demonstrated protocol (CG000375-RevC). Library preparation was
819 done following manufacturer's instructions. Libraries were sequenced on NextSeq (Illumina).
820 The raw fastq files were processed with Cell Ranger 3.0.2 (RNAseq) or Cell Ranger ARC 2.0
821 (Multiome) from 10x Genomics to generate a sparse matrix of features by barcodes. For single
822 cell mutiomic data, alignment was performed using a custom reference package containing
823 annotations for GFP and RFP genes. This output was then loaded into R version 4.0.2 and

824 processed with the R package Seurat 4.0.0(63). The data was then filtered with standard quality
825 control to remove cells with few genes expressed or an overrepresentation of mitochondrial
826 reads. Data was then scaled and normalized. Linear reduction analysis was performed by
827 calculation of PCA from the most variable genes. Cells were then clustered using a resolution of
828 0.5 and visualized by UMAP. Marker genes were used to identify different cell types present.
829 IFN/AP and Hypoxia scores were generated using the AddModuleScore function, with a control
830 value of 5. Tumor cells were binned into deciles by IFN/AP score, and Hypoxia score was then
831 plotted for each decile with the DotPlot function. Dropout events in RNA assay from multiomic
832 data were recovered using a method based on low-rank approximation (cite
833 https://www.nature.com/articles/s41467-021-27729-z). Tumor cells were characterized by the
834 expression of RFP or GFP markers and binned into deciles by Hypoxia score. Hypoxic tumor
835 cell were defined as cells in the top Hypoxia decile (top 10%) and moderate hypoxic cells as
836 cells in decile 8 and 9. Then IFN/AP score was plotted for each group with the VlnPlot function
837 and wilcox statistical test was applied using R package ggsignif 0.6.4.
838
839 **Fluorescent immunohistochemistry**
840 Primary tumors and lungs were fixed in 4% PFA for 4.5 hours, washed three times with cold
841 PBS and cryoprotected in PBS with 30% sucrose at 4ºC overnight. Tissues were then embedded
842 in OCT, frozen using dry ice/ethanol baths and stored at -80ºC. Cryosections were incubated at
843 4ºC overnight with antibodies against GFP (Abcam, ab13970), RFP (Abcam, ab62341),
844 pimonidazole (Hypoxyprobe, Pab2627), and CRE (Millipore, mab3120). The secondary
845 antibodies used in this study were Goat anti-Chicken IgY Alexa Fluor 488 (Life Technologies,
846 A11039), Goat anti-Rabbit IgG Alexa Fluor 594 (Life Technologies, A11012) and Goat anti-

847 mouse IgG Alexa Fluor 647 (Life Technologies, A21240). All secondary antibodies were
848 incubated for one hour at room temperature. Images were taken on a Keyence BZ-9000 or an
849 Axioimager A1 (Zeiss) fluorescence microscope.
850
851 **Gene expression profiling**
852 Integrity of RNA extracted with Quick-RNA MicroPrep (Zymo) was measured using
853 Bioanalyzer (Agilent). Sequencing libraries were prepared with KAPA stranded RNA-Seq Kit
854 with RiboErase (Kapa Biosystems) according to manufacturer's instructions, and single-end 75
855 bp sequencing was performed at the USC Molecular Genomics Core, using a NextSeq high
856 output 75 cycle kit (Illumina). Reads were trimmed for Nextera and Illumina adapter sequences
857 using trimgalore(64) with default parameters. Trimmed reads were mapped to hg19 (GRCh37)
858 reference using STAR (v2.7.1a)(65), and the reads mapped to the genes annotated in the
859 ENSEMBL GRCh37.p13 GTF (release 75) were quantified using HTSeq-count (v0.11.2)(66).
860 Differentially expressed genes across hypoxia-normoxia conditions were identified after
861 controlling for cell line and batch effects (FDR≤0.05), using DESeq2 (v1.26.0)(67). PCA and
862 heatmaps were generated using variance stabilizing transformed normalized counts after
863 regressing out the batch effects using removeBatchEffect function from limma package
864 (v3.42.2)(68). Pathway analysis was performed using Ingenuity Pathway Analysis (QIAGEN,
865 https://www.qiagenbioinformatics.com/products/ingenuitypathway-analysis) and overlapping
866 gene sets were found using Gene Set Enrichment Analysis at https://www.gsea-
867 msigdb.org/gsea(69,70).
868 RNA-Seq data of different breast cancer cell lines were obtained from Gene Expression
869 Omnibus (GEO). Genes differentially expressed in responder cell lines (MCF7, T47D, and

870 BT4774) compared to non-responder cell lines (231 and HS578T) were identified using DESeq2
871 after controlling for cell lines differences and study specific difference at their respective GSE
872 level. Microarray expression data of mouse Py117 and Py8119 cancer cells were
873 obtained from (GSE118181)(71). Differentially expressed (DE) genes between responsive and
874 non-responsive clones were identified using limma(68) at an FDR level of 0.05. After mapping
875 RefSeq IDs to ENSEMBL IDs, common orthologous DE genes in responder RNA-seq breast
876 cancer cell lines and mouse Py117 were identified from the two analysis.
877
878 **qRT-PCR**
879 Total RNA extracted with Quick-RNA MicroPrep (Zymo) was reverse transcribed using iScript
880 Reverse Transcription Supermix (Bio-Rad), according to the manufacturer's instructions. Real
881 time PCR was performed on a CFX96^{TM} Real-Time PCR detection system (Bio-Rad), using
882 iTaq^{TM} Universal SYBR® Green Supermix (Bio-Rad). The primer sequences used were human
883 IFIT1 (forward, 5'-AGAAGCAGGCAATCACAGAAAA-3'; reverse, 5'-
884 CTGAAACCGACCATAGTGGAAAT-3'); human IFIT3 (forward, 5'-
885 'AGGCTCTGGAAGAAAAGCCC-3', reverse, 5'-TTCTGCAGTTTCAGGCCCAA-3'); human
886 ISG15 (forward, 5-'GTACAGGAGCTTGTGCCGTG-3'; reverse, 5'-
887 ACACCTGGAATTCGTTGCCC-3'); human OAS1 (forward, 5'-
888 TGTCCAAGGTGGTAAAGGGTG-3'; reverse, 5'-CCGGCGATTTAACTGATCCTG-3'
889 human CA9 (forward, 5'-GGGTGTCATCTGGACTGTGTT-3'; reverse, 5'-
890 CTTCTGTGCTGCCTTCTCATC-3'); human PHD3 (forward, 5'-
891 GGCTGGGCAAATACTACGTCAA-3'; reverse, 5'-CCTGTTCCATTTCCCGGATAG-3');
892 human NDRG1 (forward, 5'-GTCCTTATCAACGTGAACCCTT-3'; reverse, 5'-

893 GCATTGGTCGCTCAATCTCCA-3'); human ESR1 (forward, 5'-
894 GTGGGATACGAAAAGACCGA-3'; reverse, 5'-AAGGTTGGCAGCTCTCATGT-3'); human
895 PS2 (forward, 5'- TCGGGGTCGCCTTTGGAGCAG-3'; reverse, 5'-
896 GAGGGCGTGACACCAGGAAAACCA-3'); human 36B4 (forward, 5'-
897 GTGTTCGACAATGGCAGCAT-3'; reverse, 5'-AGACACTGGCAACATTGCGGA-3');
898 mouse ifit1 (forward, 5'-TCTGCTCTGCTGAAAACCCAG-3'; reverse, 5'-
899 CAAGGAACTGGACCTGCTCTG-3'); mouse isg15 (forward, 5'-
900 GAGCTAGAGCCTGCAGCAAT-3'; reverse, 5'-TCACGGACACCAGGAAATCG-3'); mouse
901 ca9 (forward, 5'-TCTGAAGACAGGATGGAGGAGT-3'; reverse, 5'-
902 AGAGTAGGGTGCCTCCATAG-3'); mouse phd3 (forward, 5'-
903 GGGACAGGTTATGTTCGCCA-3'; reverse, 5'-TGCGGTCTGACCAGAAGAAC-3'); mouse
904 36B4 (forward, 5'-CTCGTTGGAGTGACATCGTCT-3'; reverse, 5'-
905 GTCTGCTCCCACAATGAAGC-3'). The relative RNA levels were calculated using the DDCq
906 method, using 36B4 as reference gene.
907

908 **Western blotting**

909 Cells were washed with PBS and lysed in Laemmli buffer (50 mM Tris, pH6.8, 1.25% sodium
910 dodecyl sulfate, 15% glycerol). Cell lysates were heated at 95ºC for 15 minutes for complete
911 lysis and denaturalization, after which proteins were quantified by Lowry protein assay (Bio-
912 Rad) and 5% (v/v) β-mercaptoethanol (Sigma) and 0.004% (w/v) bromophenol-blue (Sigma)
913 were added. Proteins were run on 4-15% SDS-polyacrylamide gradient gels (Bio-Rad) and
914 transferred to a low-fluorescence PVDF membrane (Millipore). Primary antibodies used in this
915 study are HIF1α (BD Biosciences, 610958), HIF2α (R&D, AF2886), ARNT (Cell Signaling,

916 5537), H3 (Abcam, ab1791), H3K4me3, (Epigentek, A-4033), H3K9me2 (Abcam, ab1220),
917 H3K9me3 (Epigentek, A-4036), H3K27me3 (Millipore, 07-449), H3K36me3 (Epigentek,
918 A4042), H3K27ac (Active Motif, 39133), IRF3 (Cell Signaling, 10949), FOXO1 (Cell
919 Signaling, 2880), FOXA1 (Abcam, ab23738), FOXO3a (Cell Signaling, 2497), and β-actin
920 (Sigma, A5441). Membranes were probed at 4ºC overnight, followed by incubation with an
921 IRDye®-conjugated anti-mouse (LI-COR, 926-32210), anti-rabbit (LI-COR, 926-68071) or anti-
922 goat secondary (LI-COR, 926-32214) antibodies and images were acquired with a LI-COR
923 Odyssey CLx Near-Infrared Fluorescence Imaging System. Alternatively, anti-mouse-HRP
924 (BioRad, 1706516) or anti-rabbit-HRP (Jackson Labs, 711035152) antibodies were used.
925
926 **Statistical analysis**
927 Results represent mean±SEM, unless otherwise indicated. Statistical significance between two
928 groups was determined by unpaired Student's t-test or Mann-Whitney test, or ANOVA for more
929 than 2 groups followed by Fisher's LSD test. Statistical analysis was done with GraphPad Prism
930 v.9.
931

FIGURE 1

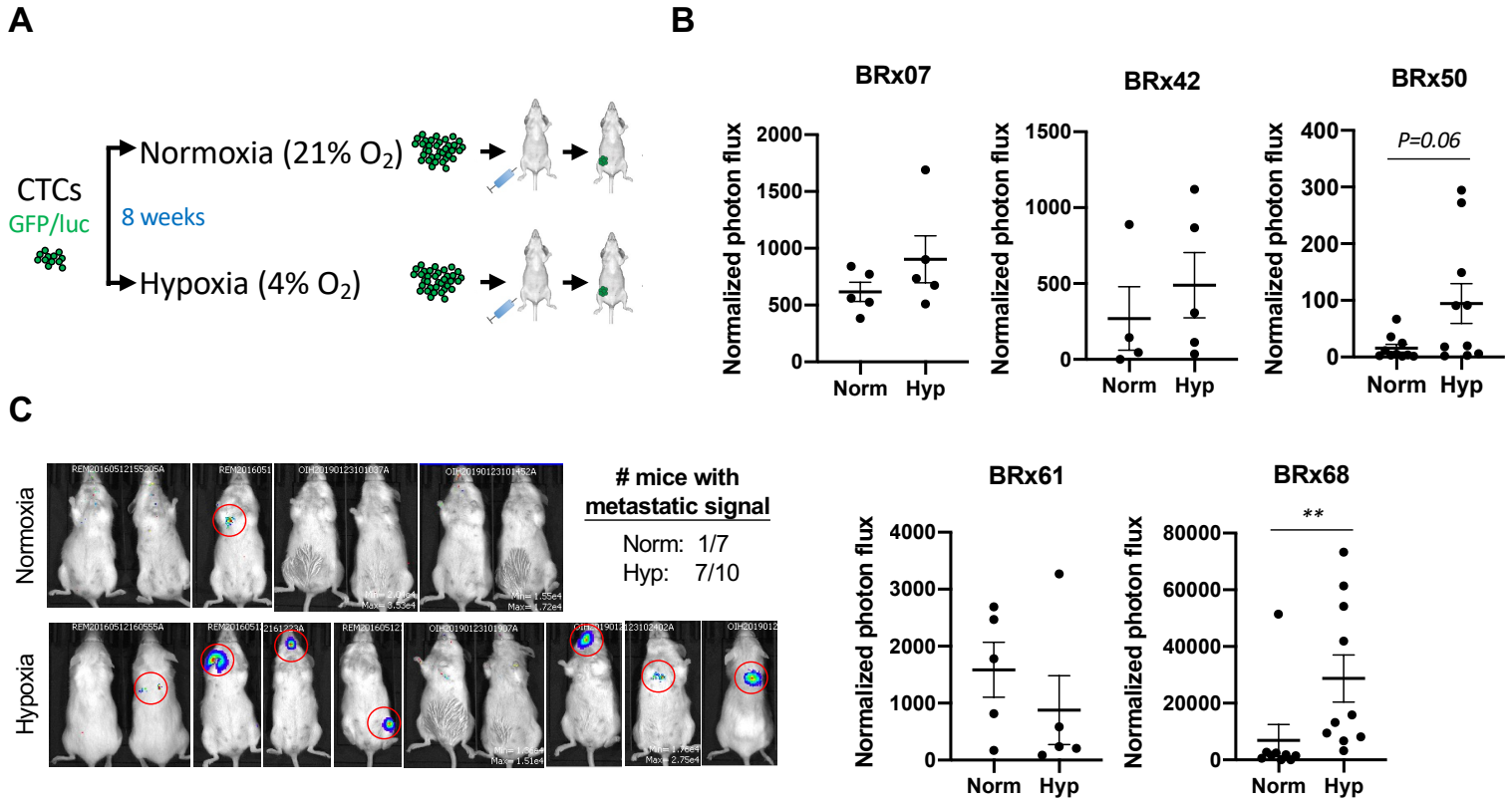
A
CTCs
GFP/luc
8 weeks
Normoxia (21% O2)
Hypoxia (4% O2)
B
BRx07
BRx42
BRx50
Normalized photon flux
Norm
Hyp
P=0.06
C
Normoxia
Hypoxia
mice with metastatic signal
Norm: 1/7
Hyp: 7/10
BRx61
BRx68
**

Figure 1: Hypoxia promotes primary tumor growth and metastasis formation in certain breast cancer CTC lines.

(A) Schematic representation of xenotransplantation experiments. Cells constitutively expressing GFP and luciferase (GFP/luc) were grown in normoxia or hypoxia for 8 weeks and injected into the 4th mammary fat pads or tail veins of NSG mice. **(B)** Tumor growth in mice orthotopically injected with different CTC lines (2,000 cells per mouse for BRx07, BRx61 and BRx68, 20,000 cells per mouse for BRx42 and BRx50), measured by bioluminescence. Normalized photon flux at 12 weeks after injection. Means ±SEM are shown. n = number of mice. P values were obtained with 2-tailed Mann-Whitney test. *P<0.05, **P<0.01. **(C)** Bioluminescence imaging data of mice 14 weeks after intravenous injection of 100,000 BRx68-GFP/luc cells per mouse.

FIGURE 2

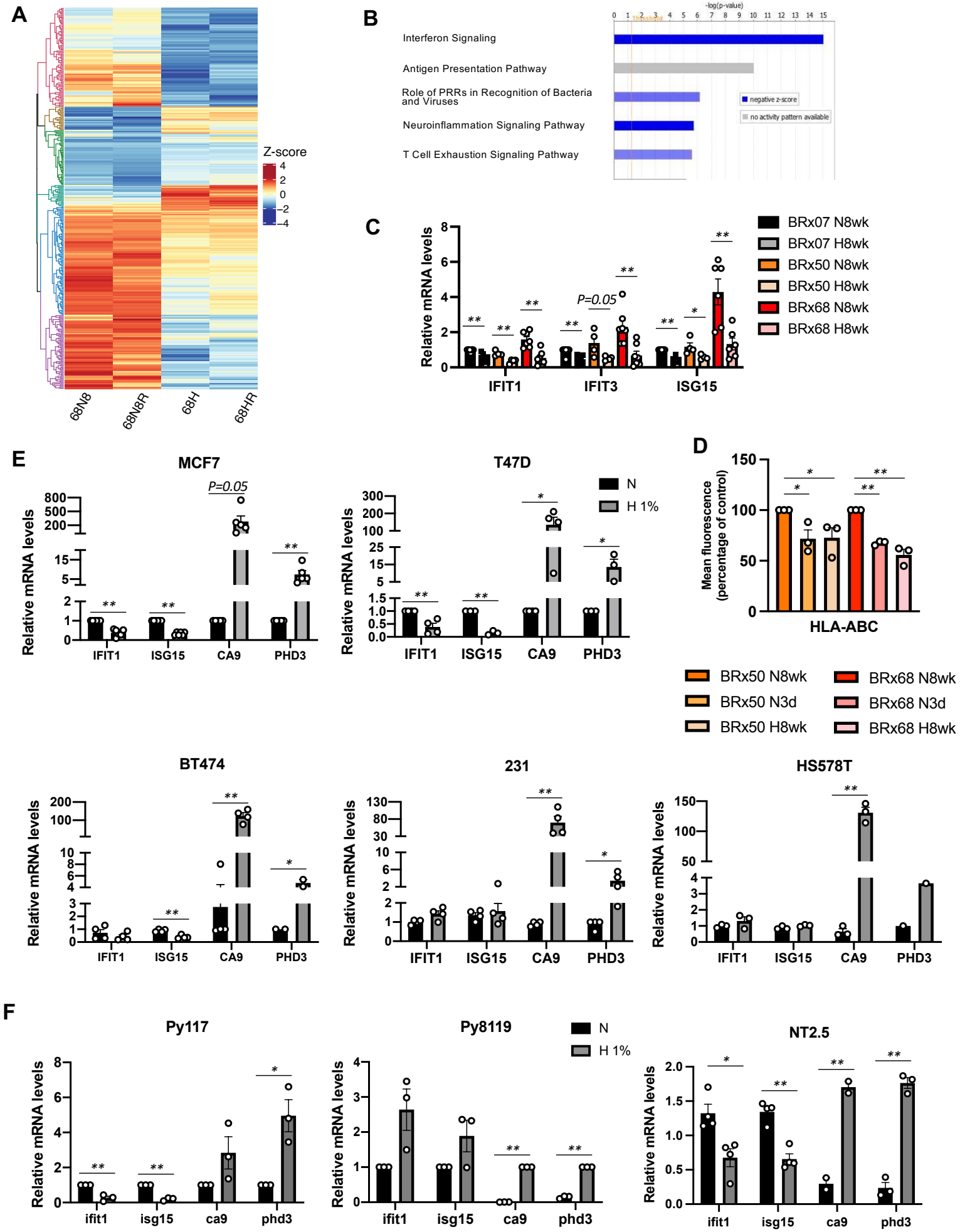
A
Z-score
4
2
0
−2
−4
68N8
68N8R
68H
68HR
B
-log(p-value)
Threshold
Interferon Signaling
Antigen Presentation Pathway
Role of PRRs in Recognition of Bacteria and Viruses
Neuroinflammation Signaling Pathway
T Cell Exhaustion Signaling Pathway
negative z-score
no activity pattern available
C
Relative mRNA levels
P=0.05
IFIT1
IFIT3
ISG15
BRx07 N8wk
BRx07 H8wk
BRx50 N8wk
BRx50 H8wk
BRx68 N8wk
BRx68 H8wk
E
MCF7
T47D
N
H 1%
Relative mRNA levels
P=0.05
IFIT1
ISG15
CA9
PHD3
D
Mean fluorescence (percentage of control)
HLA-ABC
BRx50 N8wk
BRx50 N3d
BRx50 H8wk
BRx68 N8wk
BRx68 N3d
BRx68 H8wk
BT474
231
HS578T
Relative mRNA levels
IFIT1
ISG15
CA9
PHD3
F
Py117
Py8119
NT2.5
N
H 1%
Relative mRNA levels
ifit1
isg15
ca9
phd3

Figure 2: Hypoxia downregulates type I IFN and AP pathways in luminal breast cancer cells. **(A)** Heatmap depicting genes differentially expressed in BRx68 cells grown in normoxia (N) or hypoxia (H, 4% O_2) for 8 weeks. **(B)** Top canonical pathways enriched in genes differentially expressed in BRx68 cells cultured in normoxia or hypoxia (4% O_2). Graph shows -log(p-value). Blue bar indicates negative z-score. **(C)** qPCR analysis of 3 IFN target genes in CTC lines grown in normoxia or hypoxia (4% O_2) for 8 weeks. Means ±SEM of 7 (BRx07 and BRx68) or 4 (BRx50) experiments are shown. P value was calculated with 2-tailed Student's *t* test. *P<0.05, **P<0.01. **(D)** Flow cytometry analysis of relative level of HLA-ABC in BRx68 and BRx50 cells cultured for 8 weeks in normoxia (N8), 3 days in normoxia (N3), and 8 weeks in hypoxia (H8). Means ±SEM, n=3, P value was calculated with one-way ANOVA followed by Fisher's LSD test. *P<0.05, **P<0.01. **(E-F)** qPCR analysis of 2 IFN target genes (IFIT1, ISG15) and 2 HIF target genes (CA9, PHD3) in different breast cancer cell lines of human **(E)** or mouse **(F)** origin cultured in normoxia or hypoxia (1% O_2) for 3 days. Means ±SEM. P values were calculated with 2-tailed Student's *t* test * p<0.05, ** p<0.01.

FIGURE 3

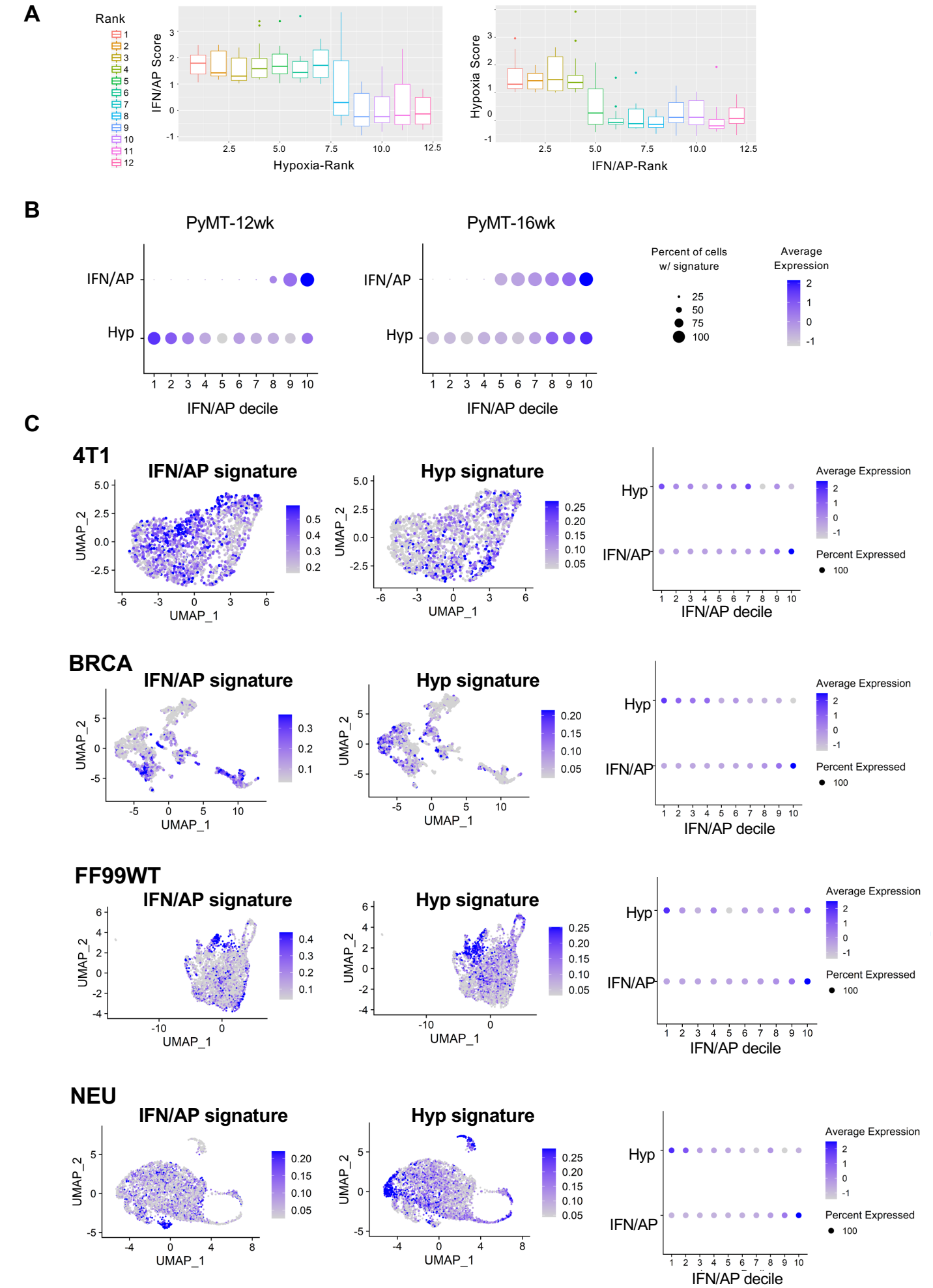
A
Rank
1
2
3
4
5
6
7
8
9
10
11
12
IFN/AP Score
Hypoxia-Rank
Hypoxia Score
IFN/AP-Rank
B
PyMT-12wk
PyMT-16wk
IFN/AP
Hyp
IFN/AP decile
Percent of cells w/ signature
25
50
75
100
Average Expression
C
4T1
BRCA
FF99WT
NEU
IFN/AP signature
Hyp signature
UMAP_1
UMAP_2
Average Expression
Percent Expressed

Figure 3: Inverse correlation of hypoxia and IFN/AP signatures in *in vivo* breast tumors and tumor cells of mouse mammary tumors.

(A) Graph illustrating inverse correlation between hypoxia signature and IFN/AP signature in breast tumors from TCGA. Tumors with detectable scores of hypoxia signature or IFN/AP signature based on RNA-seq analysis were plotted according to the hypoxia score rank (X-axis, Hypoxia-Rank) and IFN/AP Score (Y-axis) or vice versa. **(B)** Decile maps of tumor cell population based on hypoxia and IFN/AP scores for MMTV-PyMT tumors at 12 weeks or 16 weeks. Cell deciles were ranked by IFN/AP scores. **(C)** UMAP plots (left) and decile maps (right) of tumor cell population based on IFN/AP and hypoxia scores for murine breast cancer syngeneic models. Cell deciles were ranked by IFN/AP scores.

FIGURE 4

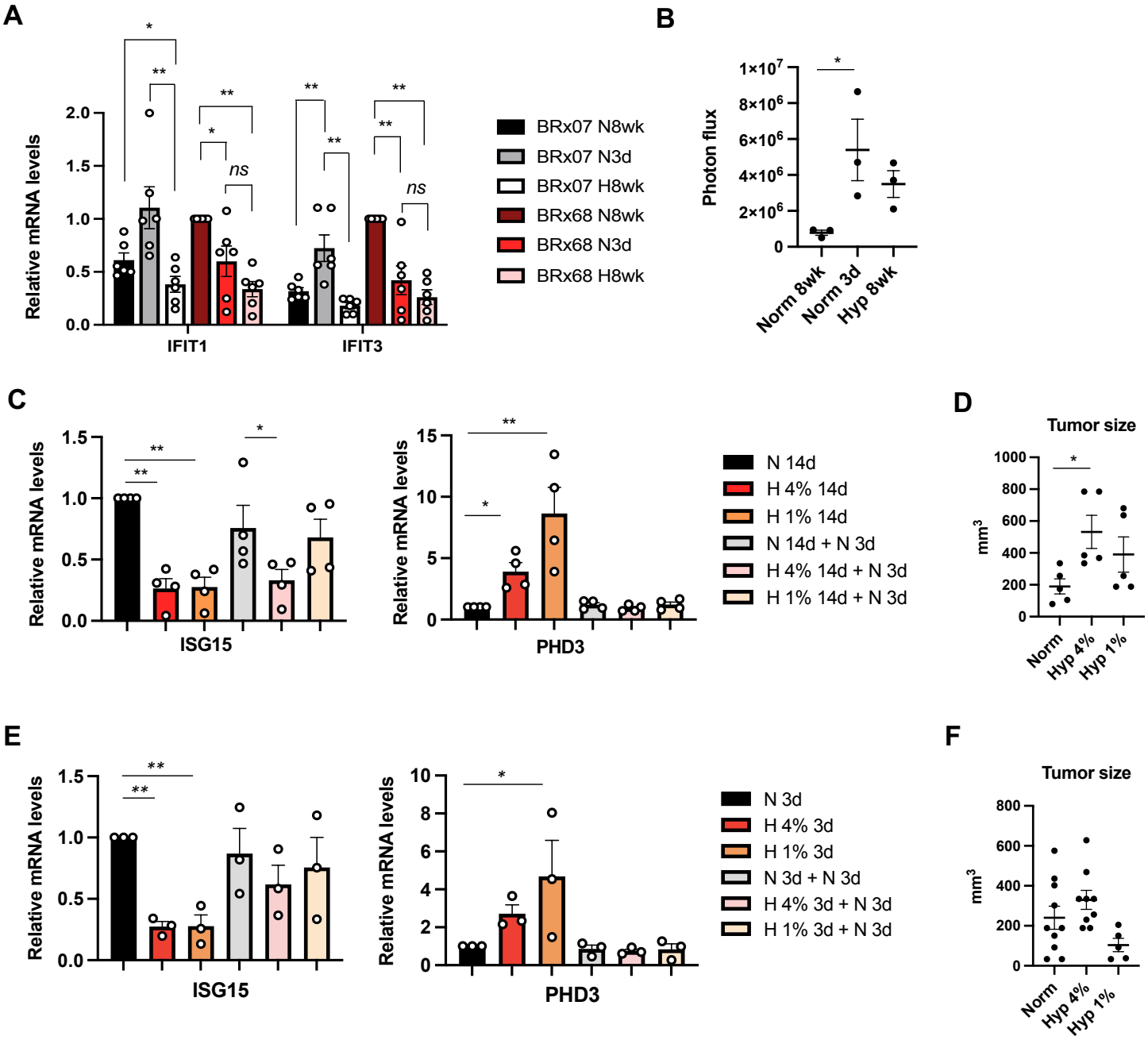
A
Relative mRNA levels
IFIT1
IFIT3
ns
BRx07 N8wk
BRx07 N3d
BRx07 H8wk
BRx68 N8wk
BRx68 N3d
BRx68 H8wk
B
Photon flux
Norm 8wk
Norm 3d
Hyp 8wk
C
ISG15
PHD3
N 14d
H 4% 14d
H 1% 14d
N 14d + N 3d
H 4% 14d + N 3d
H 1% 14d + N 3d
D
Tumor size
mm3
Norm
Hyp 4%
Hyp 1%
E
N 3d
H 4% 3d
H 1% 3d
N 3d + N 3d
H 4% 3d + N 3d
H 1% 3d + N 3d
F

Figure 4: Hypoxic memory of type I IFN suppression is associated with enhanced tumorigenesis and metastasis.

(A) Relative mRNA expression levels of IFIT1 and IFIT3 in BRx07 and BRx68 cells grown in hypoxia for 8 weeks (4% O_2, H8), or in normoxia for 8 weeks (N8) or 3 days (N3). Means ±SEM, n=6, P value was obtained with one-way ANOVA followed by Fisher's LSD test. *P<0.05, ** P<0.01. **(B)** Bioluminescence values from primary tumors 6 weeks after orthotopic injection of 2,000 BRx68-GFP/luc cells. Prior to injection, cells were grown in hypoxia (4% O_2) for 8 weeks, normoxia for 8 weeks, or normoxia for 3 days. Means ±SEM, n=3. P values were calculated with one-way ANOVA followed by Fisher's LSD test. *P<0.05. **(C)** qPCR analysis of relative mRNA expression levels of the IFN target ISG15 and the hypoxia target PHD3 in MCF7 cells grown in normoxia or hypoxia (4% O_2 or 1% O_2) for 14 days followed by an additional 3 days of reoxygenation. Means ±SEM, n=4. P values were obtained with one-way ANOVA followed by Fisher's LSD test. *P<0.05, ** P<0.01. **(D)** Tumor volumes formed by MCF7 cells cultured in normoxia or hypoxia (4% or 1%) for 14 days. Means ±SEM, n=5, P values were obtained with one-way ANOVA followed by Fisher's LSD test. *P<0.05. **(E)** qPCR analysis of relative mRNA expression levels of the IFN target ISG15 and the hypoxia target PHD3 in MCF7 cells grown in normoxia or hypoxia (4% O_2 or 1% O_2) for 14 days followed by an additional 3 days of reoxygenation. Means ±SEM, n=4. P values were obtained with one-way ANOVA followed by Fisher's LSD test. *P<0.05, ** P<0.01. **(F)** Tumor volumes formed by MCF7 cells cultured in normoxia or hypoxia (4% or 1%) for 14 days. Means ±SEM, n=5, P values were obtained with one-way ANOVA followed by Fisher's LSD test. *P<0.05.

FIGURE 5

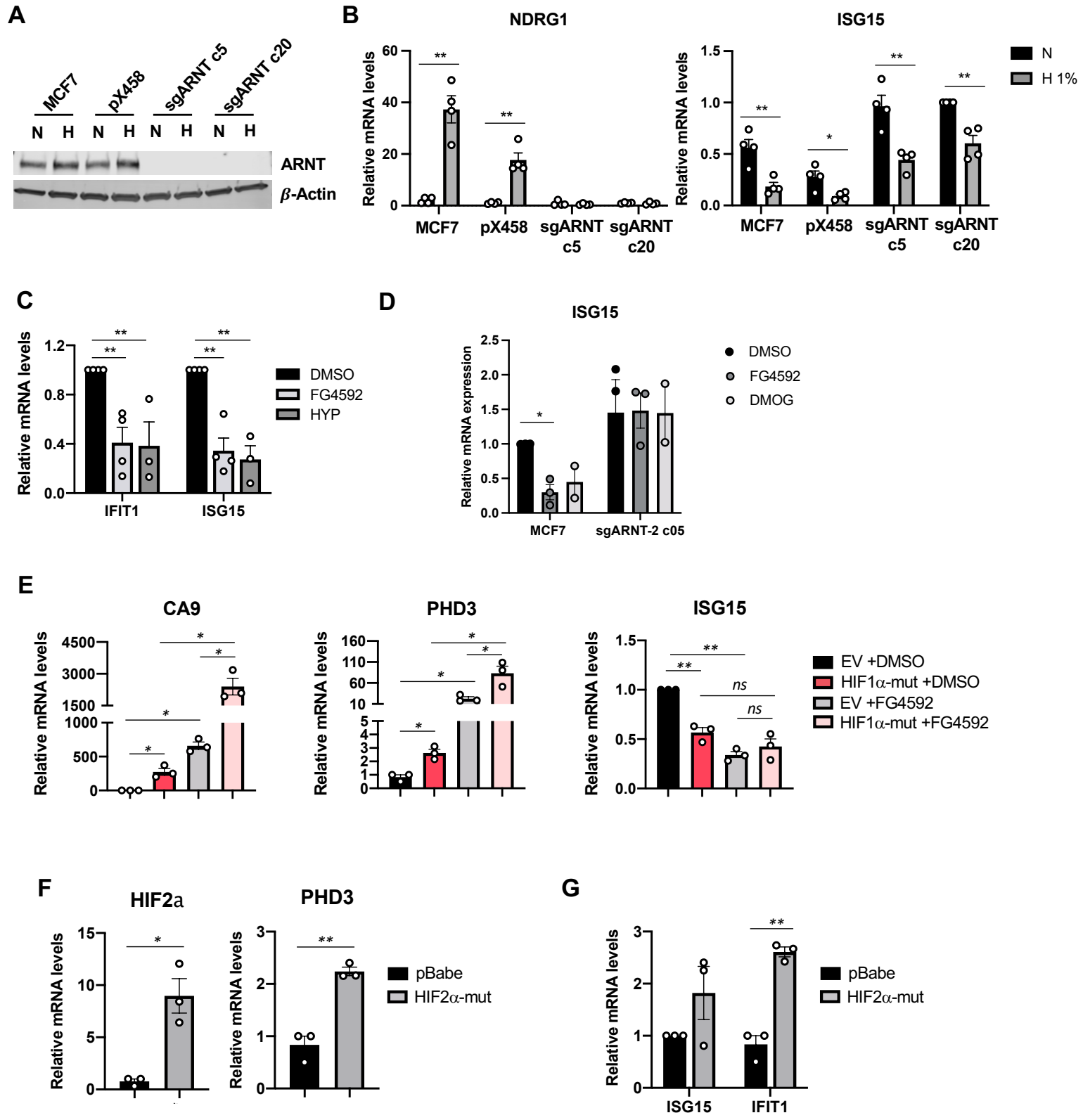
A
MCF7
pX458
sgARNT c5
sgARNT c20
N H N H N H N H
ARNT
β-Actin
B
NDRG1
ISG15
Relative mRNA levels
MCF7
pX458
sgARNT c5
sgARNT c20
N
H 1%
C
Relative mRNA levels
IFIT1
ISG15
DMSO
FG4592
HYP
D
ISG15
Relative mRNA expression
MCF7
sgARNT-2 c05
DMSO
FG4592
DMOG
E
CA9
PHD3
ISG15
Relative mRNA levels
EV +DMSO
HIF1α-mut +DMSO
EV +FG4592
HIF1α-mut +FG4592
ns
F
HIF2a
PHD3
Relative mRNA levels
pBabe
HIF2α-mut
G
Relative mRNA levels
ISG15
IFIT1
pBabe
HIF2α-mut

Figure 5: HIF-dependent and -independent mechanisms regulate IFN suppression.

(A) Immunoblot analysis of ARNT expression in ARNT-KO MCF7 cells, bulk MCF7 and a px458 control MCF7 cells. β-ACTIN is shown as a loading control. **(B)** Relative mRNA expression levels of NDRG1 (left) and ISG15 (right) in bulk MCF7 cells, 1 px458 control MCF7 clone and 2 ARNT-KO MCF7 clones grown in normoxia or hypoxia (1% O_2) for 3 days. Means ±SEM, n=4. P values were obtained with one-way ANOVA followed by Fisher's LSD test. **(C)** IFIT1 and ISG15 expression levels in MCF7 cells treated with the PHD inhibitor FG4592 (100 μM) or hypoxia for 3 days. Means ±SEM, n=4. P values were obtained with one-way ANOVA followed by Fisher's LSD test. *P<0.05, ** P<0.01. **(D)** ISG15 expression levels in MCF7 cells, or MCF7 ARNT-ko cells treated with the PHD inhibitor FG4592 (100 μM) or DMOG for 3 days. Means ±SEM, n=3 for FG4592, n=2 for DMOG. P values were obtained with one-way ANOVA followed by Fisher's LSD test. *P<0.05. **(E)** Relative mRNA expression levels of CA9 (left), PHD3 (middle) and ISG15 (right) in T47 cells with EV, HIF1α-mutant expression, treated with DMSO or FG4592 in normoxia culture for 3 days. Means ±SEM, n=3. P values were obtained with one-way ANOVA followed by Fisher's LSD test. *P<0.05, **P<0.01. **(F)** Relative mRNA expression levels of HIF2α (left), PHD3 (middle) and ISGs (right) in MCF7 cells with pBabe-EV or HIF2α-mutant expression in normoxia culture for 3 days. Means ±SEM, n=3. P values were obtained with one-way ANOVA followed by Fisher's LSD test. *P<0.05, **P<0.01.

FIGURE 6

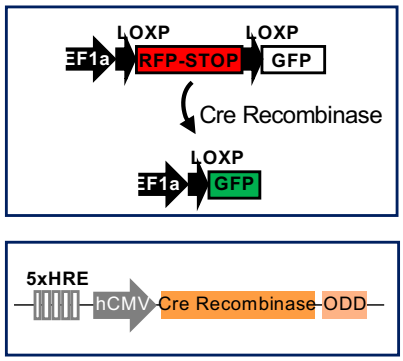
A
LOXP
LOXP
EF1a
RFP-STOP
GFP
Cre Recombinase
LOXP
EF1a
GFP
5xHRE
hCMV
Cre Recombinase
ODD

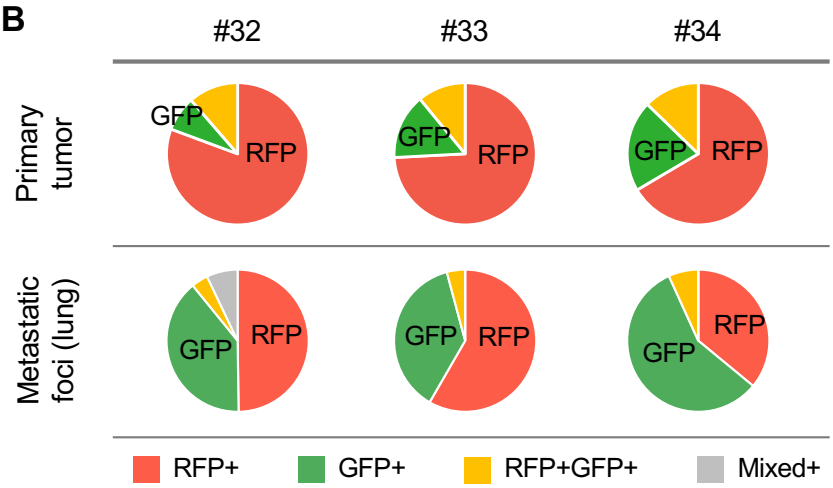
B
#32
#33
#34
Primary tumor
Metastatic foci (lung)
GFP
RFP
RFP+
GFP+
RFP+GFP+
Mixed+

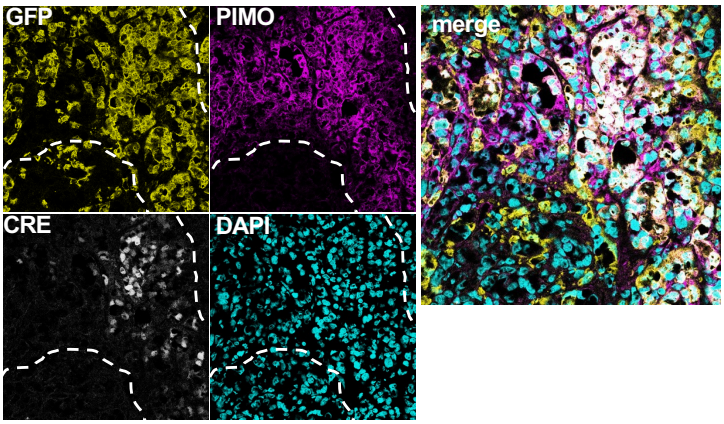
C
GFP
PIMO
merge
CRE
DAPI

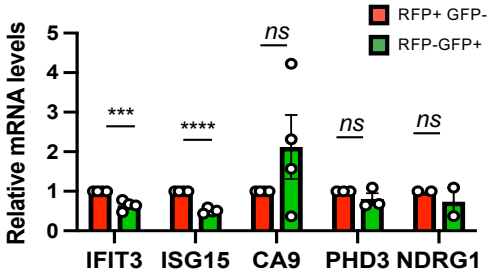
D
Relative mRNA levels
RFP+ GFP-
RFP-GFP+
***
****
ns
ns
ns
IFIT3
ISG15
CA9
PHD3
NDRG1

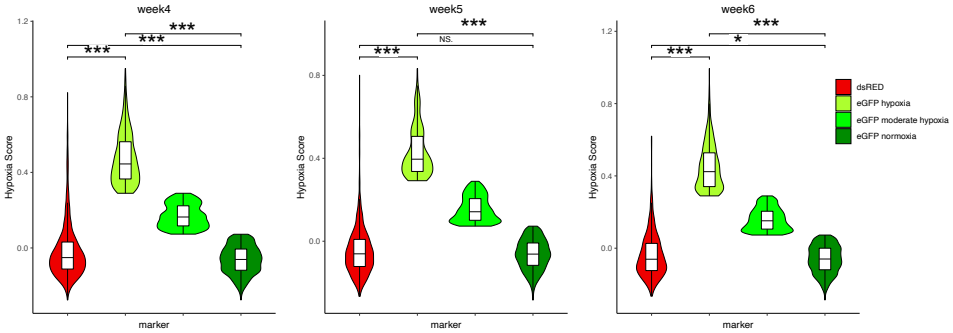
E
week4
week5
week6
Hypoxia Score
marker
NS.
dsRED
eGFP hypoxia
eGFP moderate hypoxia
eGFP normoxia

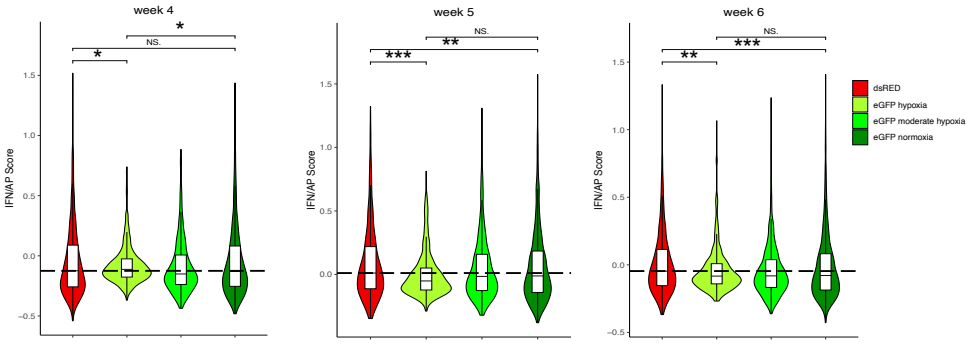
F
week 4
week 5
week 6
IFN/AP Score
NS.
dsRED
eGFP hypoxia
eGFP moderate hypoxia
eGFP normoxia

Figure 6: Hypoxia-tracing reporter system showed tumor cells with hypoxic memory and enhanced metastatic capacity.

(A) Schematic representation of the plasmids used to create the hypoxia tracing MCF7-HypT cells. **(B)** Quantification of RFP and GFP positive area in primary tumors (top) and metastatic loci in lungs (bottom). Mouse number is labeled on the top. **(C)** Representative fluorescent images of a MCF7-HypT tumor section stained with antibodies against GFP (green), pimonidazole (white) and Cre (red). Nuclei were stained with DAPI (blue). Dotted line contours the hypoxic region. Scale bars = 100 µm. **(D)** Relative mRNA levels of IFN targets (IFIT3 and ISG15) and hypoxia targets (CA9, PHD3 and NDRG1) in $RFP^{+}GFP^{-}$ and $RFP^{-}GFP^{+}$ cell populations sorted from MCF7-HypT tumors. Means ±SEM, n=4, P values were obtained with 2-tailed Student's t test. *P<0.05, ns: no significance. **(E-F)** Violin plots of hypoxia score **(E)** and IFN/AP score **(F)** from the scRNAseq data in RFP (dsRED), eGFP-hypoxia, eGFP-moderate hypoxia, eGFP-normoxia cells at week 4, 5 and 6. *P<0.05, **P<0.01, ***P<0.001. NS: not significance.

FIGURE 7

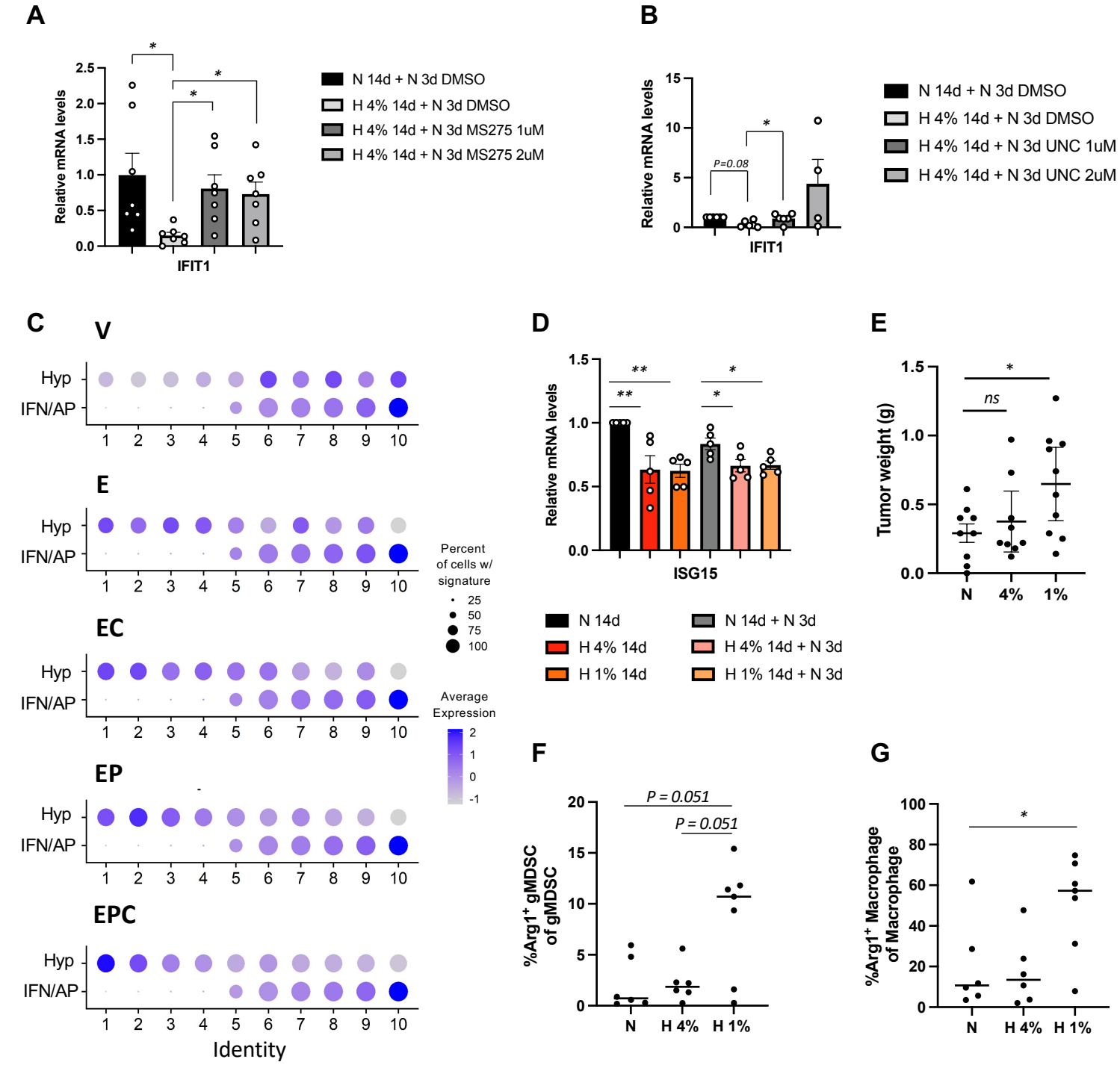
A
Relative mRNA levels
IFIT1
N 14d + N 3d DMSO
H 4% 14d + N 3d DMSO
H 4% 14d + N 3d MS275 1uM
H 4% 14d + N 3d MS275 2uM
B
Relative mRNA levels
P=0.08
IFIT1
N 14d + N 3d DMSO
H 4% 14d + N 3d DMSO
H 4% 14d + N 3d UNC 1uM
H 4% 14d + N 3d UNC 2uM
C
V
E
EC
EP
EPC
Hyp
IFN/AP
Identity
Percent of cells w/ signature
Average Expression
D
Relative mRNA levels
ISG15
N 14d
H 4% 14d
H 1% 14d
N 14d + N 3d
H 4% 14d + N 3d
H 1% 14d + N 3d
E
Tumor weight (g)
ns
N
4%
1%
F
%Arg1+ gMDSC of gMDSC
P = 0.051
P = 0.051
N
H 4%
H 1%
G
%Arg1+ Macrophage of Macrophage
N
H 4%
H 1%

Figure 7: An HDAC inhibitor can erase hypoxic memory and enhance immune clearance of tumor cells in normoxic regions.

(A-B) Relative mRNA expression levels of IFIT1 in MCF7 cells in reoxygenation experiment (primed in normoxia or hypoxia for 14 days and then reoxygenated in normoxia for 3 days) with or without MS275 **(A)** or UNC0638 **(B)**. n=7, mean±SEM, statistical significance was calculated with Brown-Forsythe and Welch's ANOVA test followed by unpaired t-test with Welch's correction, *p<0.05. **(C)** scRNAseq analysis of hypoxia and IFN/AP scores in tumor cells in the syngeneic mammary tumors formed by NT2.5 cells, treated with vehicle (V), Entinostat (E), Entinostat combined with anti-CTLA4 antibody (EC), with anti-PD1 antibody (EP), or with both (EPC). Decile plot of hypoxia and IFN/AP scores for cell population ranked based on IFN/AP scores. **(D)** Relative mRNA expression levels of isg15 in NT2.5 cells cultured in normoxia, 4% or 1% hypoxia for 14 days, and reoxygenated for 3 days. Means ±SEM, n=5, Statistical significance was calculated with one-way ANOVA followed by Fisher's LSD test. *P<0.05, ** P<0.01. **(E)** Graph showing weight of the orthotopic tumors formed by NT2.5 cells injected into FVB mice at 8 weeks. Means ±SEM. n=9 (Norm), n=9 (Hyp 4%) and n=10 (Hyp 1%). Statistical significance was calculated with one-way ANOVA followed by Fisher's LSD test. *P<0.05. **(F-G)** Graph showing percentage of Arg+ gMDSCs **(F)** and Arg+ macrophages **(G)** in the same tumors formed by NT2.5 cells in (**E**). Statistical significance was calculated with nonparametric Mann-Whitney U test. *P<0.05. **(H)** Graph illustrating a proposed model of hypoxia mediated suppression of IFN/AP and the hypoxic memory.